#270970 and +182870]) and spinocerebellar ataxia type 5 (SCA5 [MIM #600224]), respectively.[8,10,11] The α-II spectrin is considered as the major α spectrin expressed in nonerythroid cells, and α-II/β-II spectrin heterodimers are the predominant species in these cells.[9,12] Abnormal development of nodes of Ranvier and destabilizing initial clusters of voltage-gated sodium channels (VGSC) were observed in zebrafish α-II spectrin mutants harboring a nonsense mutation. The mutants also showed impaired myelination in motor nerves and in the dorsal spinal cord, suggesting that α-II spectrin plays important roles in the maintenance of the integrity of myelinated axons.[13]

Here, we describe three cases of early-onset WS with cerebral hypomyelination harboring *SPTAN1* (MIM *182810) aberrations. Two individuals with in-frame mutations showed more severe phenotypes than one individual with *SPTAN1* and *STXBP1* deletion. In-frame mutations of *SPTAN1* result in aggregation of α-II (mut)/β-II and α-II (mut)/β-III spectrin heterodimers, suggesting dominant-negative effects of the mutations. Spectrin aggregation is associated with disturbed clustering of VGSC and an elevated action potential threshold. Our findings revealed essential roles of α-II spectrin in human brain development and suggest that abnormal AIS is possibly involved in pathogenesis of infantile epilepsy.

## Subjects and Methods

### Subjects

Subjects 1, 2, and 3 have been originally reported as three of four individuals with early onset WS, severe hypomyelination, reduced white matter, and developmental delay (group A: subjects 1, 2, and 3 were previously named as No. 2, No. 1, and No. 3, respectively, and No. 4 was unavailable for this study).[14] Subject 1 has been shown to possess a 9q33.3-q34.11 microdeletion including *STXBP1*.[7] Clinical information of these three subjects with *SPTAN1* aberrations is updated in Table S1 available online. We screened for *SPTAN1* mutations in a total of eight unrelated individuals with WS accompanied by severe hypomyelination without episodes of prenatal incidents or neonatal asphyxia (six males and two females, including subjects 2 and 3 of group A). Individuals with these two distinctive features (WS and severe hypomyelination) are relatively rare. These eight patients were totally different from the previously investigated 13 EIEE patients (group B).[7] Screening tests for metabolic disorders (lactate, amino acids, and uric organic acids) were normal in all subjects. *ARX* and *CDKL5* were not mutated in the six male and two female patients, respectively. The diagnosis was made on the basis of clinical features, including tonic spasms with clustering, arrest of psychomotor development, and hypsarrhythmia on electroencephalogram, as well as brain magnetic resonance imaging (MRI) findings. Experimental protocols were approved by the Committee for Ethical Issues at Yokohama City University School of Medicine. Informed consent was obtained from all individuals included in this study, in agreement with the requirements of Japanese regulations.

### Mutation Analysis

Genomic DNA was obtained from peripheral blood leukocytes by standard methods, amplified by GenomiPhi version 2 (GE Healthcare, Buckinghamshire, UK), and used for mutational screening. Exons 2 to 57, covering the *SPTAN1* coding region (of transcript variant 1, GenBank accession number NM_001130438), were screened by high-resolution melting curve (HRM) analysis as previously described.[7] In transcript variant 2 (GenBank accession number NM_003127), the only difference is that exon 37 of variant 1 was missing. PCR conditions and primer sequences are shown in Table S2. If a sample showed an aberrant melting curve shift, the PCR product was sequenced. All mutations were also verified on PCR products directly via genomic DNA (not amplified by GenomiPhi) as a template. DNAs from 250 Japanese normal controls were screened for the two in-frame *SPTAN1* mutations by HRM analysis. Normal controls which showed aberrant melting curve shift were sequenced.

### Parentage Testing

For all families showing de novo mutations, parentage was confirmed by microsatellite analysis as previously described.[7] Biological parentage was judged if more than four informative markers were compatible and other uninformative markers showed no discrepancies.

### Expression Vectors

A full-length human *SPTAN1* cDNA was prepared by PCR with first-strand cDNA derived from a human lymphoblastoid cells (LCL) and an IMAGE clone (clone ID 5211391) as a template. The obtained *SPTAN1* cDNA was sequenced and confirmed to be identical to a RefSeq mRNA (amino acids 1–2477, GenBank accession number NM_001130438) except for two synonymous base substitutions that have been registered in dbSNP as rs2227864 and rs2227862. Site-directed mutagenesis via a KOD-Plus-Mutagenesis kit (Toyobo, Osaka, Japan) was used to generate *SPTAN1* mutants including c.6619_6621 del (p.E2207 del) and c.6923_6928 dup (p.R2308_M2309 dup). A C-terminal Flag-tag was introduced by PCR. All variant cDNAs were verified by sequencing. C-terminal Flag-tagged WT and mutant *SPTAN1* cDNAs were cloned into the pCIG vector[15,16] to express C-terminal Flag-tagged α-II spectrin as well as nuclear-localized EGFP. WT and mutant *SPTAN1* cDNAs were also cloned into the pCAG-EGFP-C1 vector, in which EGFP gene and multiple cloning sites of pEGFP-C1 vector (Clontech, Mountain View, CA) are introduced into a CAG-promoter vector,[15,16] to express N-terminal EGFP-tagged α-II spectrin.

For protein expression in *Escherichia coli*, WT and mutant *SPTAN1* cDNAs (amino acids 1445–2477, the last eight spectrin repeats and the EF hand domain) were cloned into pGEX6P-3 (GE Healthcare) to generate glutathione S-transferase (GST) fusion proteins. Human *SPTBN1* cDNAs (amino acids 1–1139, GenBank accession number NM_003128, including the actin binding domain and eight spectrin repeats) were prepared by PCR via first-strand cDNA derived from a human LCL, and were cloned into pET-24a (Merck, Darmstadt, Germany) to generate His-tag fusion proteins.

### Protein Expression, Purification, and Binding Assay

Proteins were expressed in *Escherichia coli* BL21 (DE3). Bacteria were grown at 37°C in Lysogeny Broth media with 300 μg/ml ampicillin to a density yielding an absorbance at 600 nm of 0.8. Protein expression was then induced with 1 mM isopropyl-β-D-thiogalactoside (IPTG) at 20°C overnight. Cells were collected by centrifugation and lysed by sonication. Proteins were purified by

affinity chromatography with Glutathione Sepharose High Performance (GE Healthcare) for GST-α-II spectrin or HisTrap HP (GE Healthcare) for β-II spectrin-His. α-II spectrins were further purified by HiTrap Q HP (GE Healthcare) and Superdex-200 (GE Healthcare) columns in a buffer containing 150 mM NaCl, 20 mM sodium phosphate buffer (pH 7.5), and 2 mM dithiothreitol (DTT). β-II spectrin was further purified by Superdex-200 (GE Healthcare) columns in a buffer containing 1 M NaCl, 20 mM sodium phosphate buffer (pH 7.5), and 2 mM DTT.

For the GST pull-down assay to examine the assembly of α-II/β-II heterodimers, 0.5 μM GST-α-II spectrin (WT, del mut, or dup mut) or 1 μM GST were preincubated with 1 μM β-II spectrin-His for 1 hr at 4°C with gentle agitation in binding buffer containing 150 mM NaCl, 20 mM sodium phosphate buffer (pH 7.5), and 2 mM DTT. The reaction mixture (100 μl) was transferred onto an Ultrafree-MC (Millipore, Billerica, MA), containing 50 μl of a 75% slurry of Glutathione Sepharose 4B equilibrated in binding buffer, and incubated overnight at 4°C. Unbound proteins were recovered by centrifugation at 500 × g for 2 min. The beads were washed three times with the binding buffer. The bound molecules were eluted with a buffer containing 100 mM NaCl, 20 mM sodium phosphate buffer (pH 7.5), 5 mM DTT, 1 mM EDTA, and 50 mM reduced glutathione. The eluted fractions were analyzed by SDS-PAGE, and protein bands were visualized by staining with Coomassie brilliant blue. For the analytical gel filtration experiments, 3.3 μM GST-α-II spectrin (WT, del mut, or dup mut) were preincubated with or without 3.3 μM β-II spectrin-His for 3 hr at 4°C with gentle agitation in a binding buffer containing 150 mM NaCl, 20 mM sodium phosphate buffer (pH 7.5), and 2 mM DTT. The samples were analyzed by Superdex-200 column equilibrated in binding buffer. The eluted fractions were analyzed by SDS-PAGE and protein bands were visualized by staining with Coomassie brilliant blue.

### Structural Prediction

The structure of human α-II spectrin was predicted by homology modeling with Phyre,[17] based on sequence homology between human α-II spectrin (1981–2315 aa) and chicken brain alpha spectrin (1662–1982 aa) (Protein data bank ID, 1U4Q).[18] The structure and positions of mutations were illustrated by PyMOL with the crystal structure of 1U4Q.

### Circular Dichroism Measurements

For circular dichroism (CD) measurements, GST-α-II spectrin were digested with human rhinovirus 3C protease at 4°C, and then the GST-tag was removed by affinity chromatography with glutathione sepharose 4B (GE Healthcare). We measured far-UV CD spectra and estimated the secondary structure as previously described.[7] In brief, the experiments were performed in 20 mM sodium phosphate buffer (pH 7.5) containing 150 mM NaCl, 2 mM DTT with or without 1 mM $CaCl_2$, which stabilizes the structure of the EF hand domain. α-II and β-II spectrin concentration was adjusted to 1.7 μM (without $CaCl_2$) and 1.5 μM (with $CaCl_2$). Melting (transition midpoint) temperature ($T_m$) was calculated by fitting a sigmoid-function equation with KaleidaGraph (Synergy Software, Reading, PA). The data from three independent experiments were averaged and the SD was calculated. Similar results were obtained in the presence or absence of 1 mM $CaCl_2$.

### Cell Culture, Transfection, and Immunofluorescence

For primary neuronal cultures for immunofluorescence, cortexes dissected from mice (embryonic days 14 to 15) were dissociated in 0.05% trypsin-EDTA solution (Invitrogen, Carlsbad, CA), and triturated with a Pasteur pipette. The dissociated cells were plated on 200 μg/ml poly-D-lysine (Millipore)/20 μg/ml laminin (Invitrogen)-coated glass coverslips at a density of 15,000 cells/$cm^2$. Expression vectors were introduced at the time of dissociation by electroporation, with the Amaxa Mouse Neuron Nucleofector kit (Lonza, Tokyo, Japan) according to the manufacturer's protocol (Program O-005), and 2 μg plasmid DNA per condition. After cortical neurons attached to coverslips, the medium was changed from normal medium (10% FBS in DMEM) to maintaining medium (2% B27 and 1 × penicillin-streptomycin-glutamine in Neurobasal [Invitrogen]). Half of the medium was replaced with an equal volume of maintaining medium every 4 days. LCLs were grown in RPMI 1640 medium supplemented with 10% FBS, 1 × antibiotic-antimycotic (Invitrogen), and 8 μg/ml tylosin (Sigma, Tokyo, Japan) at 37°C in a 5% $CO_2$ incubator. For the immunofluorescence imaging study, LCLs were plated on coated coverslips as described above for 3–6 hr.

Neurons and LCLs were fixed with 2% paraformaldehyde in PBS for 15 min and permeabilized with 0.1% Triton X-100 for 5 min. For detection of VGSCs, cells were fixed with methanol at −20°C for 10 min. Cells were then blocked with 10% normal goat serum for 30 min. Primary antibodies used for the study were shown in figure legends. Secondary antibodies, highly purified to minimize cross-reactivity, were used: Alexa-488-conjugated goat anti-mouse, anti-rabbit, and anti-chicken (Invitrogen), and Cy3-conjugated goat anti-mouse, anti-rabbit, and anti-chicken (Jackson ImmunoResearch, West Grove, PA). Coverslips were mounted with Vectashield (Vector Laboratories, Burlingame, CA) that contained 4,6-diamidino-2-phenylindole (DAPI) and visualized with an AxioCam MR CCD fitted to Axioplan2 fluorescence microscope (Carl Zeiss, Oberkochen, Germany). We captured images with Axio Vision 4.6 software (Carl Zeiss). Immunofluorescence of aggregated mutant α/β spectrins was much brighter than WT α/β spectrins, leading to constant short exposure time compared with the WT. For detection of ankyrinG and VGSCs, the exposure time was fixed in a series of experiments in order to enable direct comparison between different samples. For evaluation of ankyrinG and VGSC expression, 50 isolated transfected neurons were analyzed in each experiment, and representative cells were photographed. The results were confirmed at least in three independent experiments.

### Electrophysiology

Mouse neocortices at embryonic day 15 were dissociated and plated on poly-L-lysine-coated plastic coverslips (Cell desk LF, MS-0113L; Sumitomo Bakelite, Tokyo, Japan) at a density of about 100,000 cells/$cm^2$. 1 μg of expression vector for either WT, del mut, or dup mut α-II spectrin was introduced at the time of dissociation by electroporation with an Amaxa Mouse Neuron Nucleofector kit (Lonza). Primary cortical neurons were cultured in neurobasal medium supplemented with B27 and penicillin-streptomycin-glutamine (Invitrogen). During the culture period, one-half of the medium was changed every day. Whole-cell patch-clamp recordings were obtained from mice neocortical neurons at 9 days in vitro (DIV) neuronal culture. A coverslip was assembled to recording chambers on the stages of upright microscopes (Olympus, Tokyo, Japan) and continuously perfused with oxygenated, standard artificial cerebrospinal fluid (ACSF) at a flow rate of 2 ml/min and a temperature of 30°C. The standard ACSF solution contained the following (mM): 126 NaCl, 2.5 KCl,

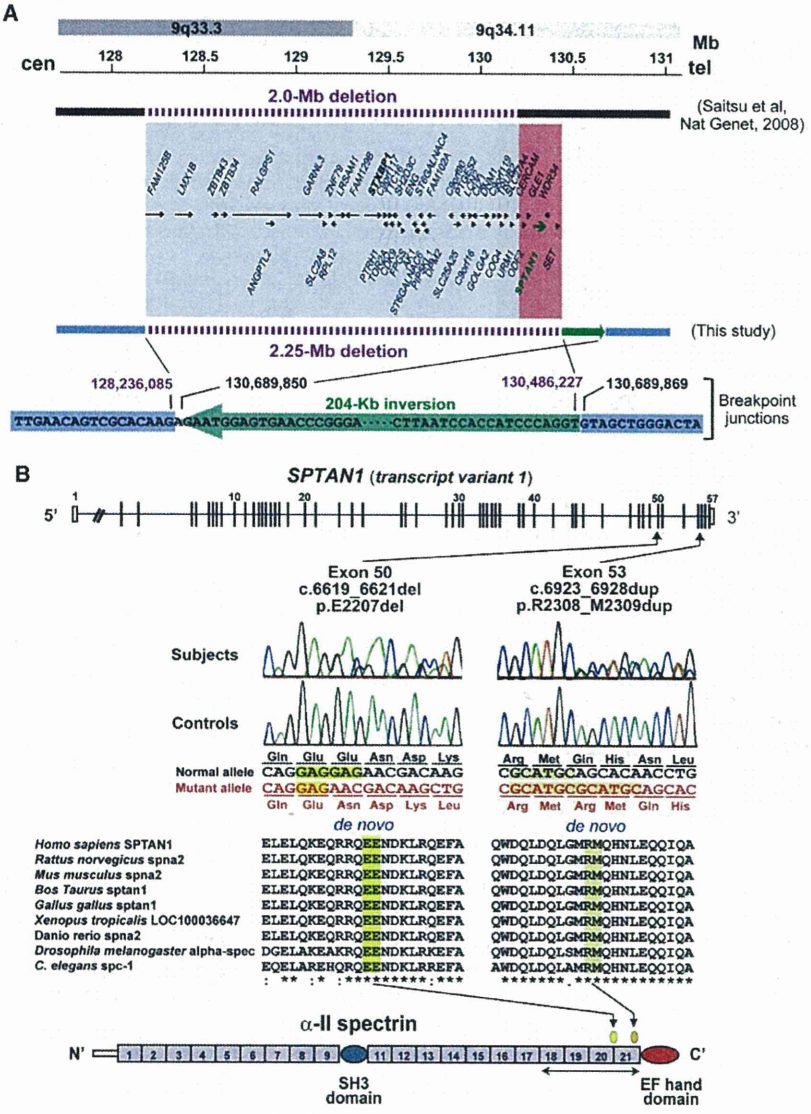


**Figure 1. *SPTAN1* Aberrations in Individuals with West Syndrome and Cerebral Hypomyelination**

(A) Genomic rearrangements at 9q33.3-q34.11 in subject 1. Top depicts chromosomal bands and genomic location (Mb) from the p telomere (cen, toward the centromere; tel, toward the telomere). Our previous study by BAC array could reveal the approximate size of the deletion (2.0 Mb) (horizontal line above boxes).[7] The deletion was newly analyzed by Affymetrix GeneChip 250K array and turned out to be 2.25 Mb in size (chr9:128,236,086-130,486,226) (UCSC genome browser coordinate [version Mar. 2006]) (horizontal line below boxes). Blue and red boxes indicate old and renewed deletion intervals, respectively. Five RefSeq genes (*ODF2*, *GLE1*, *SPTAN1*, *WDR34*, and *SET*) were newly found (in red box). The rearrangements include an unexpected 204 kb inversion (green arrow). Intact genomic regions are shown in sky blue.

(B) Schematic representation of *SPTAN1* (transcript variant 1) consisting of 57 exons (UTR and coding region are open and filled rectangles, respectively). Exon 37 of transcript variant 1 is missing in variant 2, the only difference between the two transcripts. Two distinct mutations were found at evolutionary conserved amino acids in triple helical repeats (spectrin repeats). All these mutations occured de novo. Homologous sequences were aligned with the CLUSTALW web site. α-II spectrin consists of 22 domains (numbered), including 20 spectrin repeats, an SH3 domain, and an EF hand domain. The mutations occurred within the last four spectrin repeats, which are required for α/β heterodimer association (bidirectional arrow).

1.25 $NaH_2PO_4$, 2.0 $MgSO_4$, 2.0 $CaCl_2$, 26.0 $NaHCO_3$, and 20.0 glucose. The images of cells were acquired with Olympus BX51 or BX61 microscopes equipped with electron-multiplying CCD (EMCCD) cameras, #C9100-13 or #C9100-02 (Hamamatsu Photonics, Hamamatsu, Japan), respectively. Transfected cells were selected for recordings by their fluorescence in the nucleus via a 40× water-immersion objective lens (UMPlanFI, Olympus). Membrane currents and membrane potentials were recorded with an Axopatch 700A and 200B amplifier, respectively. Signals were low-pass filtered at 10 kHz and digitized at 50 kHz by means of Digidata 1332A data-acquisition system (Molecular Devices, Tokyo, Japan). Passive membrane properties and action potentials were recorded with patch pipettes (5.8–8.0 MΩ) filled with the following intercellular solutions (in mM): 130 K-methanesulfonic acid, 10 KCl, 2 $MgCl_2$, 0.1 EGTA, and 10 HEPES (pH 7.3) with KOH. For current clamp experiments, cells were held at −60 mV by constant current injection as needed, and their firing pattern were recorded in response to sustained depolarizing current injections (500 ms duration, +10 pA increments) to analyze the input-output relationship in each cell. A single action potential was also evoked to determine their firing threshold. The injection current amplitude (10 ms duration) was increased in 2–10 pA increments from a subthreshold to an intensity well beyond threshold. Voltage-clamp studies for sodium currents were carried out with patch pipettes (5.8–8.0 MΩ) filled with the following intercellular solutions (mM): 145 tetraethylammonium-Cl, 15 NaCl, 2 $MgCl_2$, 10 EGTA, 10 HEPES, 3 MgATP, and 0.4 GTP (pH 7.4) with NaOH. Series resistance was usually below 20 MΩ and compensated by 70%–80%. The remaining linear capacitive and leakage currents were subtracted off-line by scaling average traces recorded at hyperpolarized voltages. Voltage-dependent inward sodium currents were elicited by 500 ms depolarizing steps in 5 mV increments from −90 to +10 mV at a holding membrane potential of −90 mV. For measuring the inactivation protocol of sodium currents, 500 ms long prepotentials started at − 90 mV and were incremented by 5 mV steps while the command potential was kept constant at −30 mV. The current elicited during each test pulse was normalized to the maximal current (I/Imax). Statistical

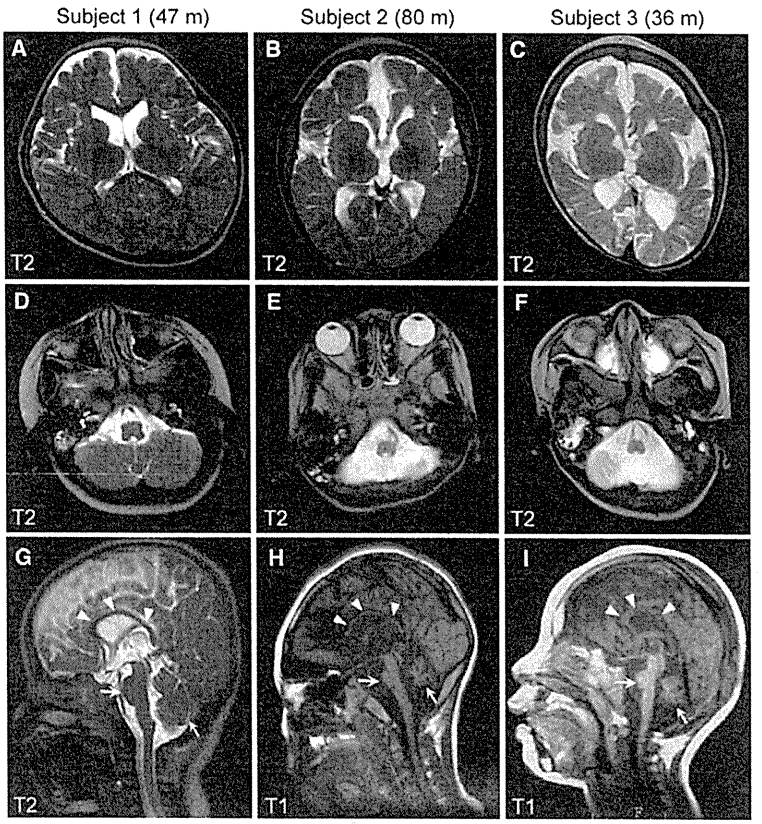


**Figure 2. Brain MRI of Subjects with *SPTAN1* Aberrations at the Most Recent Developmental Stages**

(A–C) T2-weighted axial images through the basal ganglia. Subject 1 (with a 2.25 Mb deletion) showed only slightly reduced white matter (A). By contrast, cortical atrophy and severe hypomyelination with strikingly reduced volume of white matter were evident, especially in the frontal lobes, in subjects with in-frame mutations (subjects 2 and 3) (B and C).

(D–I) T2-weighted axial images through the brainstem/cerebellum (D–F) and T2- (G) or T1-weighted midline sagittal images (H and I). Compared with subject 1 (D and G), subjects 2 (E and H) and 3 (F and I) show a thinned and shortened corpus callosum (arrowheads), severe atrophy of the brainstem, and hypoplasia and/or atrophy of the cerebellar hemispheres and vermis (arrows). m, months.

analyses were made with two-way repeated-measures ANOVA followed by a Bonferroni post-test for analysis of the input-output relationship and current amplitude at every voltage step. One-way ANOVA followed by Dunnet's posthoc test was applied for threshold, peak current, kinetics of action potentials, and passive membrane properties. The results are given as mean ± SEM, and threshold p value for statistical significance was 0.05. Statistical comparisons were performed with the Prism 4.0 (GraphPad software, La Jolla, CA).

## Results

### Identification of *SPTAN1* In-Frame Mutations

We previously reported a de novo 9q33.3-q34.11 microdeletion involving *STXBP1* in an individual with EIEE, who transited afterward to WS at the age of 3 months (subject 1).[7] Subject 1 was originally reported as one of four individuals (group A) who showed early onset WS and severe cerebral hypomyelination (as patient No. 2).[14] It is likely that haploinsufficiency of *STXBP1* caused EIEE and subsequent WS in subject 1;[7] however, no mutations of *STXBP1* were found in two of the remaining three individuals of group A (subjects 2 and 3, previously described as No. 1 and No. 3, and No. 4 was unavailable for this study).[14] Based on obvious severe hypomyelination of the group A individuals, we hypothesized that another gene within the deletion may contribute to the phenotype of group A, especially for severe hypomyelination. Re-examination of the deletion interval by genomic microarray and long PCR successfully determined the 2.25 Mb deletion and the associated 204 kb inversion (Figure 1A and see Figure S1). Among the 46 genes mapped within the deletion, *SPTAN1*, which encodes α-II spectrin, appeared to be a primary candidate because zebrafish α-II spectrin mutants showed impaired myelination.[13] We found de novo heterozygous mutations in *SPTAN1* in subjects 2 and 3 (parentage was confirmed in their respective families). Subject 2 has an in-frame 3-bp deletion (c.6619_6621 del) leading to p.E2207 del in the continuous helix region between the last two spectrin repeats, and subject 3 has an in-frame 6 bp duplication (c.6923_6928 dup, p.R2308_M2309 dup) within the last spectrin repeat (Figure 1B). These two mutations were absent in 250 Japanese normal controls (500 alleles). *SPTAN1* was further screened in six unrelated individuals with WS and hypomyelination similar to the phenotype of group A (not belonging to group B), but no mutations were found.

### Phenotypes Associated with *SPTAN1* Aberrations

The clinical features of the three subjects with *SPTAN1* aberrations are summarized in Table S1. Subjects 2 and 3 showed severe spastic quadriplegia, no developmental progress, and poor visual attention. Epileptic seizures were resistant to various treatments. Subject 3 died of fulminant myocarditis at 3 years of age. In contrast, subject 1 showed slight psychomotor development with eye contact, but no head control. Her seizures have been well controlled. Brain MRI of subjects 2 and 3 revealed widespread brain atrophy including brainstem, hypoplasia, and/or atrophy of the cerebellar hemispheres and vermis, ventriculomegaly, a thinned and shortened corpus callosum, and severe hypomyelination with strikingly reduced white matter at 6 and 3 years of age, respectively (Figure 2). Of note, while subject 1 initially showed

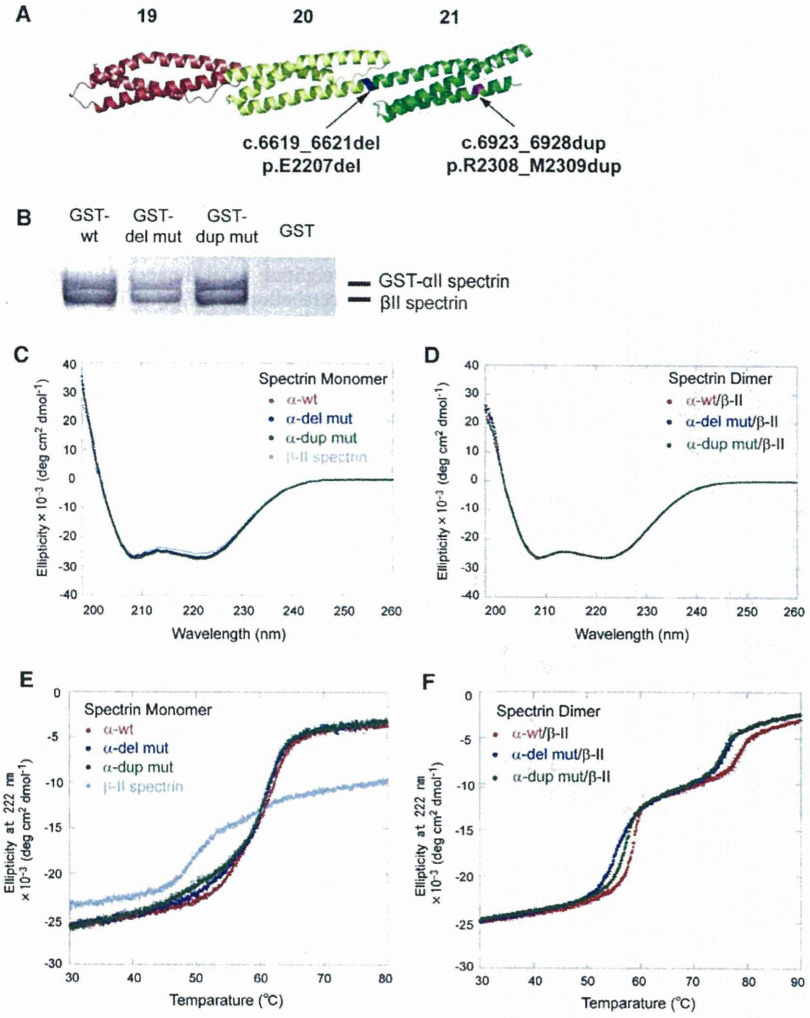


**Figure 3. Mutational Effects on the α-II/β-II Spectrin Heterodimer**

(A) Positions of the two mutations (c.6619_6621del, p.E2207 del in blue; c.6923_6928dup, p.R2308_M2309 dup in purple) in the predicted human α-II spectrin structure. Domains 19–21 (the last three spectrin repeats) are colored red, yellow, and green, respectively.

(B) GST pull-down assay of a recombinant GST-tagged α-II spectrin/β-II spectrin heterodimer. The WT and two mutant α-II spectrins could form heterodimers with β-II spectrin at comparable levels. β-II spectrin did not show any binding to GST alone.

(C–F) CD spectra (C and D) and CD melting curves (E and F) at 222 nm of the WT, del mut, and dup mut of α-II spectrins and β-II spectrin as a monomer (C and E) and as heterodimers of the WT, del mut, and dup mut of α-II spectrins with β-II spectrin (D and F). CD spectra showed no difference in the helical content of the WT and mutant α-II spectrin monomers and heterodimers with β-II spectrin (C and D). The WT and mutant α-II spectrin monomers are unfolded at 60°C, whereas β-II spectrin is unfolded around at 50°C (E). In contrast, dimers of WT and mutant α-II spectrins with β-II spectrin are partly dissociated and accompanied with denaturation of a local part of the monomers at 50°C–60°C (*Tm* [°C]: 58.362 ± 0.059 [WT], 55.617 ± 0.047 [del mut], 57.110 ± 0.077 [dup mut]) and completely unfolded at 70°C–80°C (*Tm* [°C]: 78.515 ± 0.327 [WT], 75.813 ± 0.115 [del mut], 75.267 ± 0.469 [dup mut]) (F). The thermostability of the heterodimers is obviously different between the WT and the mutants. Each dot represents the average of three repeated experiments; error bars, SD.

striking hypomyelination of cerebral cortex and thin corpus callosum at 12 months of age,[14] she completed myelination and showed only slightly reduced white matter at 4 years of age (Figure 2). The apparent differences of drug intractability and severity of cerebral hypomyelination and brainstem/cerebellum atrophy (subjects 2 and 3 versus subject 1) strongly suggested dominant-negative, rather than loss-of-function, effects of the in-frame mutations.

### Characterization of α-II/β-II and α-II/β-III Heterodimers

The mutations were predicted to affect formation of α/β spectrin heterodimers, because they were located at the initial nucleation site of the α/β spectrin heterodimer[19] (Figures 1B and 3A). To examine the properties of the α-II spectrin mutants in the context of dimer formation, we purified recombinant WT and the two mutant α-II spectrin proteins (c.6619_6621 del, p.E2207 del and c.6923_6928 dup, p.R2308_M2309 dup, designated as del mut and dup mut, respectively). Both GST pull down and analytical gel filtration experiments revealed that the two mutants could form heterodimers with β-II spectrin at comparable levels to the WT (Figure 3B). Circular dichroism (CD) spectra indicated no difference of helical content between WT and mutant α-II spectrin monomers, nor between WT and mutant α-II/β-II heterodimers (Figures 3C and 3D). However, CD melting experiments revealed that the mutations apparently affected the thermostability of α-II/β-II heterodimers (Figure 3F). Considering the melting curves of α-II and β-II spectrin monomers (Figure 3E), the melting transitions of heterodimers in the ranges of 50°C–60°C and 70°C–80°C represent partial dissociation of heterodimers to monomers accompanied by denaturation of a local part of the monomers and complete denaturation, respectively (Figure 3F). Apparent differences of melting curves in the 50°C–60°C and 70°C–80°C ranges suggested that the mutations alter the stability of α-II/β-II heterodimers.

The effect of the mutations was further clarified by transient expression in cultured mouse cortical neurons. α-II

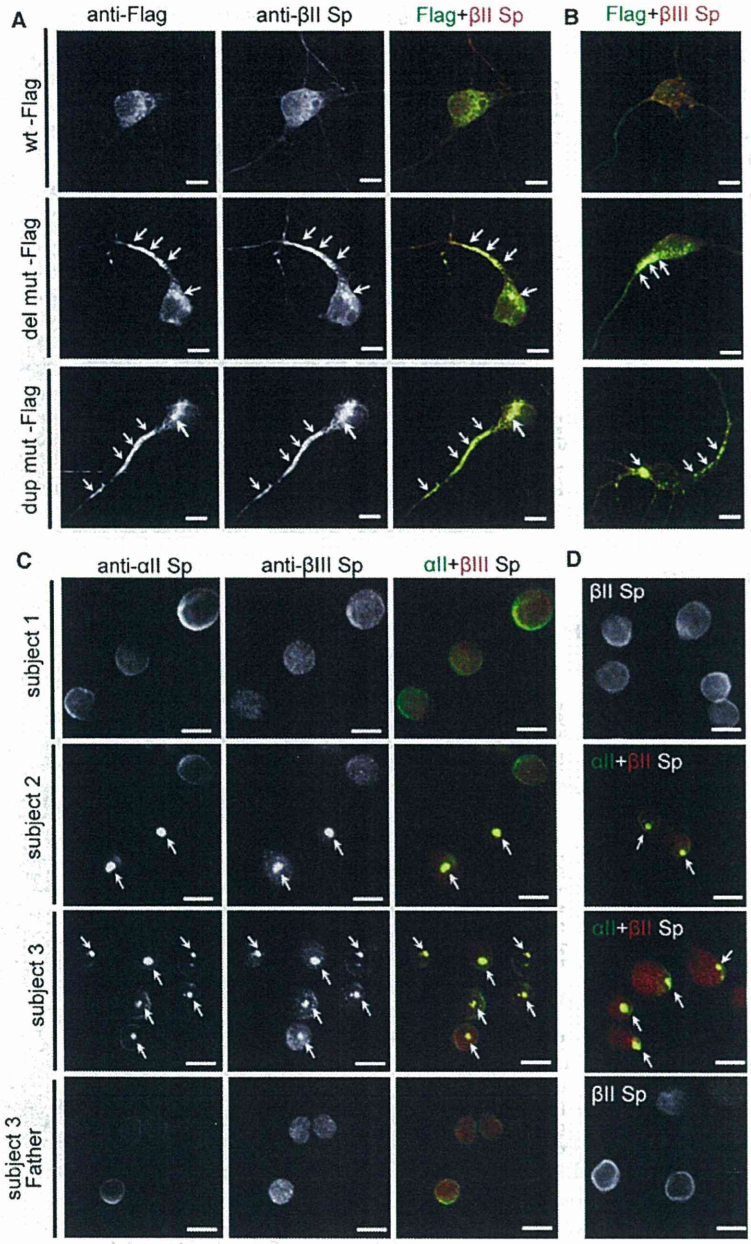


**Figure 4. Mutant α-II Spectrin Causes Aggregation of α/β Spectrin Heterodimer**

(A and B) Expression of the WT and the two mutant α-II spectrins at 7 DIV. Flag tagged-α-II spectrin (WT-Flag) showed similar expression to endogenous α-II spectrin (top, compare with Figure S2A). However, two mutant α-II spectrins (del mut-Flag and dup mut-Flag) showed aggregation predominantly in cell bodies and axons (arrows), and these aggregations were colocalized with β-II and β-III spectrins (middle and bottom). (C and D) Aggregation of endogenous α/β spectrin heterodimers were found in LCLs derived from two subjects harboring *SPTAN1* in-frame mutations. In LCLs of subject 2 (with c.6619_6621del, p.E2207del) and subject 3 (with c.6923_6928dup, p.R2308_M2309dup), aggregation of α-II/β-III (C) and α-II/β-II (D) spectrin heterodimers were frequently observed (middle two panels, arrows), while such aggregation was never observed in subject 1 (top). LCL of subject 3's father did not show any such aggregation (bottom).

The scale bars represent 10 μm. The following primary antibodies were used: mouse anti-α-II spectrin (1:400 dilution; clone D8B7; Abcam, Tokyo, Japan), mouse anti-β-II spectrin (1:600 dilution; clone 42/B-spectrin II; BD Transduction laboratories, San Jose, CA), rabbit anti-β-II spectrin (1:100 dilution; Abcam), rabbit anti-β-III spectrin (1:400 dilution; Abcam), mouse anti-Flag M2 (1:1000 dilution; Sigma), and rabbit anti-DDDDK-Tag (1:2000 dilution; MBL, Nagoya, Japan).

spectrin has been shown to be expressed in mouse brain, especially in neuronal axons.[20] In cultured cortical neurons, α-II spectrin was expressed at cell extensions and the periphery,[21] overlapping with the expression of β-II and β-III spectrins (Figure S2). We generated two α-II spectrin expression vectors: one was a dual expression vector of C-terminally Flag-tagged α-II spectrin and nuclear EGFP (Flag-nucEGFP), and the other was an N-terminally EGFP-tagged (EGFP) α-II spectrin. Tagged WT α-II spectrin from both vectors showed similar expression to endogenous α-II spectrin (Figure 4A and Figure S2). Notably, the two mutant α-II spectrins (del mut and dup mut) showed aggregation, predominantly in cell bodies and axons (Figure 4A, arrows, and Figure S2). Double immunostaining revealed that these aggregations were colocalized with β-II and β-III spectrins (Figures 4A and 4B, arrows, and Figure S2), indicating that unstable α-II/β-II and α-II/β-III spectrin heterodimers were involved in the aggregation. Remarkably, LCLs established from subjects 2 and 3 also showed similar aggregation, while LCLs of subject 1 and subject 3's parents showed no aggregation (Figures 4C and 4D, arrows). These findings indicated dominant-negative effects of the mutations for the integrity of α-II/β-II and α-II/β-III spectrin heterodimers. Immunostaining against β-IV spectrin did not show its involvement in the mutant aggregation (Figure S2).

### Effects of the *SPTAN1* Mutations on ankyrinG and VGSC Clustering at AIS

Spectrins play important roles in clustering specific integral membrane proteins at high density in specialized regions of the plasma membrane.[8] To examine the effects of α/β spectrin heterodimer impairment, protein localization at AIS was examined, where ankyrinG and VGSC are clustered and action potentials are initiated.[22,23] At 9

DIV, expression of ankyrinG and VGSC were clustered at AIS when WT Flag-nucEGFP was transfected (Figures 5A and 5B, top). In contrast, clustering of ankyrinG and VGSC was disturbed in the presence of extensive α-II (mut)/β-II and α-II (mut)/β-III spectrin aggregation (Figures 5A and 5B, middle and bottom). Interestingly, whole-cell current clamp recordings from cortical neurons expressing mutant α-II spectrins showed impairment of repetitive action potential elicitation and elevated threshold of action potential compared with those expressing the WT (Figure 6A), while there were no significant differences in the passive membrane properties among the genotypes (Table S3). Recordings of whole-cell sodium currents with conventional activation and inactivation protocols revealed that expression of the mutants caused a significant depolarizing shift in activation compared with the WT, indicating increased threshold of sodium currents (Figures 6B and 6C). These mutants did not affect any of the activation kinetic properties (10%–90% rise time) (Figure 6E), the voltage dependence of inactivation (Figures 6F and 6G), or the whole cell capacitance (Table S3). However, peak sodium current densities were substantially reduced in cells expressing dup mut or del mut (Figure 6D). Divergent distribution of VGSC at AIS can increase the action potential threshold probably resulting from the waste of charging current across the axonal membrane;[24] therefore, the abnormal spike initiation observed in two mutants could be caused by the disturbance of VGSC clustering at AIS.

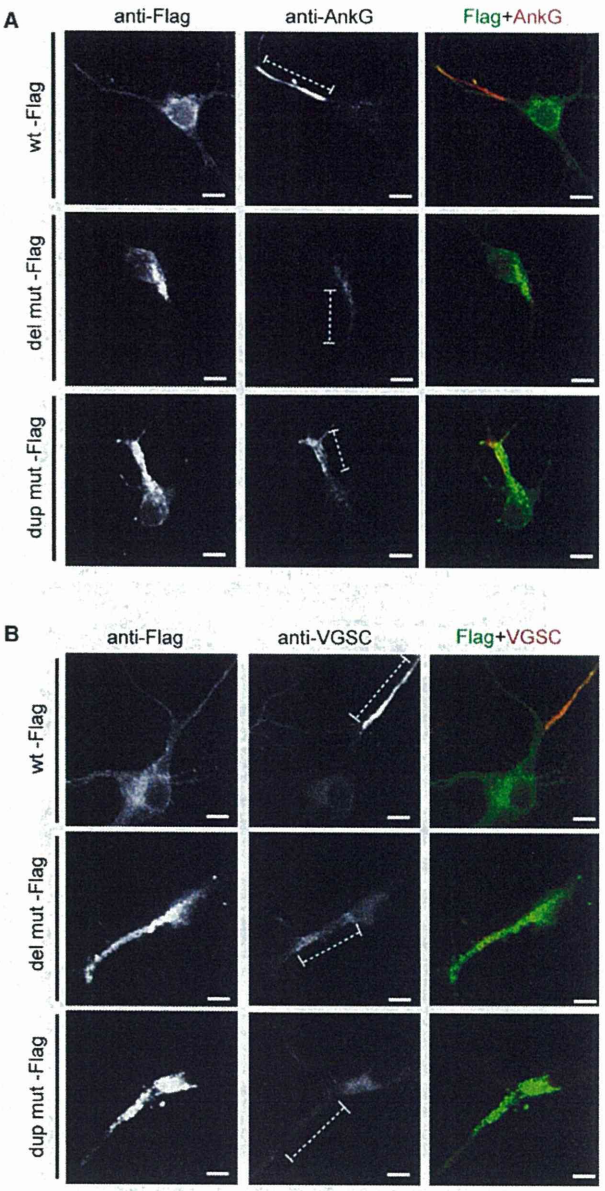


**Figure 5. Transient Expression of Mutant α-II Spectrin Led to Disturbance of AnkyrinG and VGSC Clustering at AIS**
Expression of ankyrinG (AnkG) (A) and VGSC (B) at 9 DIV. When WT α-II spectrin is expressed, neurons showed clustering of AnkG and VGSC at AIS (top). However, clustering of AnkG and VGSC were disturbed in the presence of extensive α/β spectrin aggregation when mutant α-II spectrins (both the del mut and the dup mut) were expressed (middle and bottom). AIS regions are shown by dashed lines. The scale bars represent 10 μm. The following primary antibodies were used: mouse anti-ankyrinG (1:100 dilution; clone 4G3F8; Santa Cruz Biotechnology, Santa Cruz, CA), mouse anti-pan sodium channel (for VGSC) (1:100 dilution; clone K58/35; Sigma), and rabbit anti-DDDDK-Tag (1:2000 dilution; MBL).

## Discussion

We have shown that two de novo in-frame mutations of *SPTAN1* cause early-onset WS with spastic quadriplegia, poor visual attention, and severe developmental delay. Brain MRI of the two subjects showed severe cerebral hypomyelination, decreased white matter, widespread brain atrophy including brainstem, hypoplasia and/or atrophy of the cerebellum, and a thinned and shortened corpus callosum. On the other hand, mutations of *STXBP1* cause EIEE, and brain MRI of individuals with *STXBP1* mutations showed no structural malformations in contrast with striking structural abnormalities with *SPTAN1* mutations.[7] Among three subjects harboring *SPTAN1* aberrations, subject 1 deleted both *SPTAN1* and *STXBP1* heterozygously.[7] Similar to individuals with *STXBP1* mutations, subject 1 had distinctive features of EIEE, such as early onset of spasms, suppression-burst pattern on electroencephalogram, transition to West syndrome, and severe developmental delay.[7] Therefore it is likely that haploinsufficiency of *STXBP1* caused EIEE and subsequent WS in subject 1. However, subject 1 additionally showed apparent hypomyelination of cerebral cortex and thin corpus callosum at 12 months of age,[14] which appeared to be distinct from clinical features caused by *STXBP1* mutations. Based on these differences, we hypothesized that another gene within the deletion may contribute to severe hypomyelination, and successfully found two de novo in-frame mutations of *SPTAN1* in subject 2 and 3 of

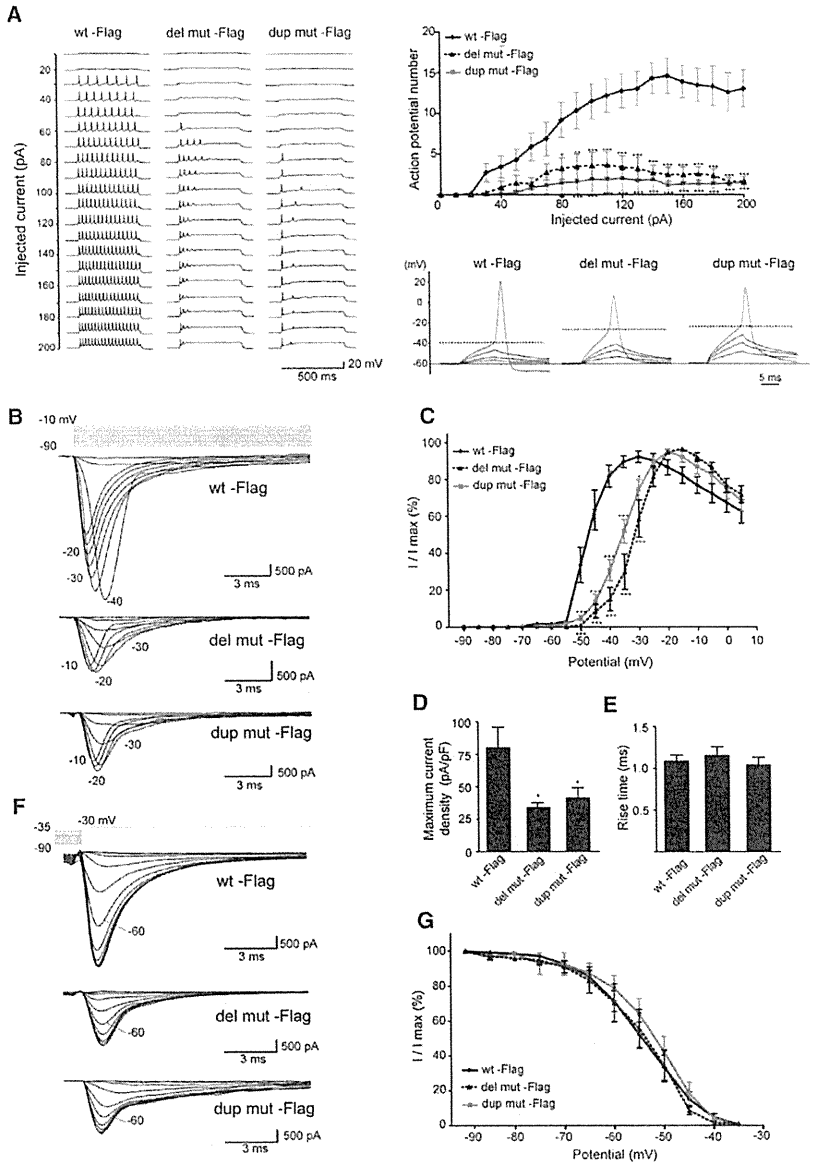


**Figure 6. Mutant α-II Spectrin Elevated Action Potential Threshold in Primary Cultured Cortical Neurons**

(A) Left, representative sets of action potential traces recorded from cultured cortical neurons expressing either WT or mutant α-II spectrin (del mut or dup mut)-Flag-nucEGFP during 500 ms injection of depolarizing current in +10 pA increments, from a holding potential of −60 mV. Right top, input-output relationship of the number of evoked action potentials versus the injected current (WT, n = 7; del mut, n = 9; dup mut, n = 7). Although there were no significant differences in the passive membrane properties among each genotypes (see Table S3), repetitive action potential elicitation was significantly reduced in the two mutants. Right bottom, representative responses to a series of subthreshold and suprathreshold depolarizing current injections of 10 ms duration. A base holding potential (−60 mV) and an identified action potential threshold are indicated by thin and dashed lines, respectively. Note that mutants elevated action potential threshold compared with the WT (see Table S3).

(B–G) Recordings of whole-cell sodium currents with conventional activation (C–E: WT, n = 11; del mut, n = 10; dup mut, n = 10) and inactivation protocols (G: WT, n = 11; del mut, n = 9; dup mut, n = 10).

(B) Representative sets of sodium current traces recorded from dissociated cortical neurons expressing WT and mutant α-II spectrins.

(C) Voltage dependence of channel activation measured during voltage steps between −90 and +10 mV. Statistical analysis indicated that del mut and dup mut exhibited significant differences in current-voltage relationship compared with the WT. Both mutants displayed a significant depolarizing shift in activation compared with the WT.

(D) Peak current density elicited by test pulses. Statistical analysis indicated a significant reduction in peak current in both mutants compared with the WT.

(E) Activation kinetics assessed by 10%–90% rise time plotted against test potential for WT and mutants. There were no significant differences among WT and the two mutants.

(F) Representative sodium currents in neurons expressing WT or mutant α-II spectrin under influence of 500 ms inactivation prepotentials.

(G) Voltage dependence of inactivation assessed in response to inactivating prepulses between −90 and −35 mV. Statistical analysis revealed no significant differences among WT and mutants ($p = 0.96$).

Error bars, SEM. *$p < 0.05$, **$p < 0.01$, ***$p < 0.001$, as compared to the WT. Most of the recorded parameters are summarized in Table S3.

group A. Although subject 1 initially showed severe hypomyelination, the myelination showed catch-up completion at 4 years of age. These facts suggest that *SPTAN1* hemizygosity may have temporary effects on the myelination. Further reports of microdeletions involving *SPTAN1* may give us a clear answer about the contribution of *SPTAN1* hemizygosity to hypomyelination. By contrast, subjects 2 and 3 showed more severe phenotypes than subject 1, indicating that the effect of in-frame mutations was dominant negative rather than loss of function. This idea was supported by the fact that the in-frame mutations could cause aggregation of α-II/β-II and α-II/β-III spectrin heterodimers, related to disturbed clustering of ankyrinG and VGSC at AIS. β-II and β-III spectrins have been shown to participate in stabilization of membrane proteins and axonal transport.[25,26] Although our study did not detect aggregation of the α-II/β-IV spectrin heterodimer, which is essential for stabilization of membrane proteins at

AIS,[27,28] defective α-II/β-II and α-II/β-III spectrin heterodimers might affect the stability of membrane proteins at AIS, possibly in combination with disrupting intracellular transport.

The α-II (mut)/β-II spectrin heterodimers was more unstable than the α-II (WT)/β-II heterodimers, which was manifested by CD melting experiments as differences of melting points at relatively high temperature (50°C–60°C and 70°C–80°C). In general, structural instability of proteins would lead to aggregate formation. Immunofluorescence analysis in both transiently transfected primary neuron and LCL derived from two subjects showed aggregation of α-II/β-II and α-II/β-III spectrin heterodimers, suggesting that structual instability of α-II/β-II and α-II/β-III spectrin heterodimers resulted in the aggregation.

We demonstrated a possible link between a mutant submenbranous scaffolding protein and abnormal AIS integrity. It has been suggested that the levels of ion channels at AIS are regulated by altering the cytoskeletal scaffolds.[22] A recessive mutation of scaffolding protein CASPR2 causes focal epilepsy.[29] Abnormal AIS integrity resulting from mutant α-II spectrin further underscores the importance of AIS scaffolds in the pathogenesis of epilepsy and provides new insights for WS.

## Supplemental Data

Supplemental Data include two figures and three tables and can be found with this article online at http://www.cell.com/AJHG.

## Acknowledgments

The authors declare no conflict of interest. We would like to thank all the patients and their families for their participation in this study. We also thank Dr. Jun-ichi Miyazaki for permitting use of CAG promoter and Dr. Sean Megason for the pCIG vector. This work was supported by research grants from the Ministry of Health, Labour, and Welfare (N.M., J.T., and M. Kato), the Japan Science and Technology Agency (N.M.), a Grant-in-Aid for Scientific Research on Priority Areas (Research on Pathomechanisms of Brain disorder) from the Ministry of Education, Culture, Sports, Science, and Technology of Japan (N.M.), a Grant-in-Aid for Scientific Research from Japan Society for the Promotion of Science (N.M. and M. Kato), a Grant-in-Aid for Young Scientist from Japan Society for the Promotion of Science (H.S.), the Research Promotion Fund from Yokohama Foundation for Advancement of Medical Science (H.S.), the Research Promotion Fund from the Uehara Memorial Foundation (H.S.), research grants from the Japan Epilepsy Research Foundation (H.S.), a grant from the 2009 Strategic Research Project of Yokohama City University (H.S.), and a research grant from the Naito Foundation (N.M.). This work has been done at Advanced Medical Research Center, Yokohama City University.

Received: March 11, 2010
Revised: April 29, 2010
Accepted: April 30, 2010
Published online: May 20, 2010

## Web Resources

The URLs for data presented herein are as follows:

ClustalW, http://align.genome.jp/
dbSNP, http://www.ncbi.nlm.nih.gov/projects/SNP/
GenBank, http://www.ncbi.nlm.nih.gov/Genbank/
Online Mendelian Inheritance in Man (OMIM), http://www.ncbi.nlm.nih.gov/Omim/
Phyre, http://www.sbg.bio.ic.ac.uk/phyre/
Protein Data Bank, http://www.pdb.org/pdb/home/home.do
PyMOL, http://www.pymol.org/
UCSC Genome Browser, http://genome.ucsc.edu/cgi-bin/hgGateway

## References

1. Kato, M. (2006). A new paradigm for West syndrome based on molecular and cell biology. Epilepsy Res. *70* (*Suppl 1*), S87–S95.
2. Bahi-Buisson, N., Nectoux, J., Rosas-Vargas, H., Milh, M., Boddaert, N., Girard, B., Cances, C., Ville, D., Afenjar, A., Rio, M., et al. (2008). Key clinical features to identify girls with *CDKL5* mutations. Brain *131*, 2647–2661.
3. Strømme, P., Mangelsdorf, M.E., Shaw, M.A., Lower, K.M., Lewis, S.M., Bruyere, H., Lütcherath, V., Gedeon, A.K., Wallace, R.H., Scheffer, I.E., et al. (2002). Mutations in the human ortholog of *Aristaless* cause X-linked mental retardation and epilepsy. Nat. Genet. *30*, 441–445.
4. Kato, M., Das, S., Petras, K., Sawaishi, Y., and Dobyns, W.B. (2003). Polyalanine expansion of ARX associated with cryptogenic West syndrome. Neurology *61*, 267–276.
5. Djukic, A., Lado, F.A., Shinnar, S., and Moshé, S.L. (2006). Are early myoclonic encephalopathy (EME) and the Ohtahara syndrome (EIEE) independent of each other? Epilepsy Res. *70* (*Suppl 1*), S68–S76.
6. Ohtahara, S., and Yamatogi, Y. (2006). Ohtahara syndrome: With special reference to its developmental aspects for differentiating from early myoclonic encephalopathy. Epilepsy Res. *70* (*Suppl 1*), S58–S67.
7. Saitsu, H., Kato, M., Mizuguchi, T., Hamada, K., Osaka, H., Tohyama, J., Uruno, K., Kumada, S., Nishiyama, K., Nishimura, A., et al. (2008). *De novo* mutations in the gene encoding STXBP1 (MUNC18-1) cause early infantile epileptic encephalopathy. Nat. Genet. *40*, 782–788.
8. Bennett, V., and Healy, J. (2008). Organizing the fluid membrane bilayer: Diseases linked to spectrin and ankyrin. Trends Mol. Med. *14*, 28–36.
9. Bennett, V., and Baines, A.J. (2001). Spectrin and ankyrin-based pathways: Metazoan inventions for integrating cells into tissues. Physiol. Rev. *81*, 1353–1392.
10. Ikeda, Y., Dick, K.A., Weatherspoon, M.R., Gincel, D., Armbrust, K.R., Dalton, J.C., Stevanin, G., Dürr, A., Zühlke, C., Bürk, K., et al. (2006). Spectrin mutations cause spinocerebellar ataxia type 5. Nat. Genet. *38*, 184–190.
11. Perrotta, S., Gallagher, P.G., and Mohandas, N. (2008). Hereditary spherocytosis. Lancet *372*, 1411–1426.
12. Meary, F., Metral, S., Ferreira, C., Eladari, D., Colin, Y., Lecomte, M.-C., and Nicolas, G. (2007). A mutant alphaII-spectrin designed to resist calpain and caspase cleavage questions the functional importance of this process in vivo. J. Biol. Chem. *282*, 14226–14237.

13. Voas, M.G., Lyons, D.A., Naylor, S.G., Arana, N., Rasband, M.N., and Talbot, W.S. (2007). alphaII-spectrin is essential for assembly of the nodes of Ranvier in myelinated axons. Curr. Biol. *17*, 562–568.
14. Tohyama, J., Akasaka, N., Osaka, H., Maegaki, Y., Kato, M., Saito, N., Yamashita, S., and Ohno, K. (2008). Early onset West syndrome with cerebral hypomyelination and reduced cerebral white matter. Brain Dev. *30*, 349–355.
15. Megason, S.G., and McMahon, A.P. (2002). A mitogen gradient of dorsal midline Wnts organizes growth in the CNS. Development *129*, 2087–2098.
16. Niwa, H., Yamamura, K., and Miyazaki, J. (1991). Efficient selection for high-expression transfectants with a novel eukaryotic vector. Gene *108*, 193–199.
17. Kelley, L.A., and Sternberg, M.J. (2009). Protein structure prediction on the Web: A case study using the Phyre server. Nat. Protoc. *4*, 363–371.
18. Kusunoki, H., Minasov, G., Macdonald, R.I., and Mondragón, A. (2004). Independent movement, dimerization and stability of tandem repeats of chicken brain α-spectrin. J. Mol. Biol. *344*, 495–511.
19. Speicher, D.W., Weglarz, L., and DeSilva, T.M. (1992). Properties of human red cell spectrin heterodimer (side-to-side) assembly and identification of an essential nucleation site. J. Biol. Chem. *267*, 14775–14782.
20. Riederer, B.M., Zagon, I.S., and Goodman, S.R. (1986). Brain spectrin(240/235) and brain spectrin(240/235E): Two distinct spectrin subtypes with different locations within mammalian neural cells. J. Cell Biol. *102*, 2088–2097.
21. Xu, J., Ziemnicka, D., Scalia, J., and Kotula, L. (2001). Monoclonal antibodies to alphaI spectrin Src homology 3 domain associate with macropinocytic vesicles in nonerythroid cells. Brain Res. *898*, 171–177.
22. Ogawa, Y., and Rasband, M.N. (2008). The functional organization and assembly of the axon initial segment. Curr. Opin. Neurobiol. *18*, 307–313.
23. Lai, H.C., and Jan, L.Y. (2006). The distribution and targeting of neuronal voltage-gated ion channels. Nat. Rev. Neurosci. *7*, 548–562.
24. Kuba, H., Ishii, T.M., and Ohmori, H. (2006). Axonal site of spike initiation enhances auditory coincidence detection. Nature *444*, 1069–1072.
25. Muresan, V., Stankewich, M.C., Steffen, W., Morrow, J.S., Holzbaur, E.L., and Schnapp, B.J. (2001). Dynactin-dependent, dynein-driven vesicle transport in the absence of membrane proteins: a role for spectrin and acidic phospholipids. Mol. Cell *7*, 173–183.
26. Kizhatil, K., Yoon, W., Mohler, P.J., Davis, L.H., Hoffman, J.A., and Bennett, V. (2007). Ankyrin-G and β2-spectrin collaborate in biogenesis of lateral membrane of human bronchial epithelial cells. J. Biol. Chem. *282*, 2029–2037.
27. Komada, M., and Soriano, P. (2002). [β]IV-spectrin regulates sodium channel clustering through ankyrin-G at axon initial segments and nodes of Ranvier. J. Cell Biol. *156*, 337–348.
28. Parkinson, N.J., Olsson, C.L., Hallows, J.L., McKee-Johnson, J., Keogh, B.P., Noben-Trauth, K., Kujawa, S.G., and Tempel, B.L. (2001). Mutant β-spectrin 4 causes auditory and motor neuropathies in quivering mice. Nat. Genet. *29*, 61–65.
29. Strauss, K.A., Puffenberger, E.G., Huentelman, M.J., Gottlieb, S., Dobrin, S.E., Parod, J.M., Stephan, D.A., and Morton, D.H. (2006). Recessive symptomatic focal epilepsy and mutant contactin-associated protein-like 2. N. Engl. J. Med. *354*, 1370–1377.

BRAIN RESEARCH 1360 (2010) 17–27

available at www.sciencedirect.com

ScienceDirect

www.elsevier.com/locate/brainres

BRAIN RESEARCH

Research Report

# Neural development of methyl-CpG-binding protein 2 null embryonic stem cells: A system for studying Rett syndrome

Yasunori Okabe[a,b,1], Akira Kusaga[a,c,1], Tomoyuki Takahashi[a,d,1], Chiaki Mitsumasu[a,c], Yoshinaka Murai[b], Eiichiro Tanaka[a,b], Hideho Higashi[b], Toyojiro Matsuishi[a,c], Ken-ichiro Kosai[a,c,e,*]

[a]Division of Gene Therapy and Regenerative Medicine, Cognitive and Molecular Research Institute of Brain Diseases, Kurume University, Kurume, Japan
[b]Department of Physiology, Kurume University of Medicine, Kurume, Japan
[c]Department of Pediatrics, Kurume University of Medicine, Kurume, Japan
[d]Department of Advanced Therapeutics and Regenerative Medicine, Kurume University of Medicine, Kurume, Japan
[e]Department of Gene Therapy and Regenerative Medicine, Advanced Therapeutics Course, Kagoshima University Graduate School of Medical and Dental Sciences, Kagoshima, Japan

ARTICLE INFO

*Article history:*
Accepted 27 August 2010
Available online 25 September 2010

*Keywords:*
MeCP2
Rett syndrome
Embryonic stem cell
Adenoviral vector

ABSTRACT

Mutations in methyl-CpG-binding protein 2 (MeCP2) gene cause the neurodevelopmental disorder Rett syndrome (RTT). Here, we describe a new experimental system that efficiently elucidates the role of MeCP2 in neural development. MeCP2-null and control ES cells were generated by adenoviral conditional targeting and examined for maintenance of the undifferentiated ES cell state, neurogenesis, and gliogenesis during *in vitro* differentiation. In addition, dopamine release and electrophysiological features of neurons differentiated from these ES cells were examined. Loss of MeCP2 did not affect undifferentiated ES cell colony morphology and growth, or the timing or efficiency of neural stem cell differentiation into Nestin-, TuJ- or TH-positive neurons. In contrast, gliogenesis was drastically accelerated by MeCP2 deficiency. Dopamine production and release in response to a depolarizing stimulus in MeCP2-null ES-derived dopaminergic neurons was intact. However, MeCP2-null differentiated neurons showed significantly smaller voltage-dependent $Na^+$ currents and A-type $K^+$ currents, suggesting incomplete maturation. Thus, MeCP2 is not essential for maintenance of the undifferentiated ES cell state, neurogenesis, or dopaminergic function; rather, it is principally involved in inhibiting gliogenesis. Altered neuronal maturity may indirectly result from abnormal glial development and may underlie the pathogenesis of RTT. These data contribute to a better understanding of the developmental roles of MeCP2 and the pathogenesis of RTT.



* *Corresponding author*. Department of Gene Therapy and Regenerative Medicine, Advanced Therapeutics Course, Kagoshima University Graduate School of Medical and Dental Sciences, 8-35-1 Sakuragaoka, Kagoshima 890-8544, Japan. Fax: +81 9 265 9721.
E-mail address: kosai@m2.kufm.kagoshima-u.ac.jp (K. Kosai).

*Abbreviations:* MeCP2, methyl-CpG-binding protein 2; RTT, Rett syndrome; BDNF, brain-derived neurotrophic factor; GFAP, glial fibrillary acidic protein; ES cells, embryonic stem cells; DNs, dopaminergic neurons; TH, tyrosine hydroxylase; HPLC, high performance liquid chromatography; ACT, adenoviral conditional targeting; NSCs, neural stem cells; TTX, tetrodotoxin; TEA-Cl, tetraethylammonium-chloride; 4-AP, 4-aminopyridine; HBSS, Hanks' balanced salt solution

[1] These authors were equally contributed to this work.

0006-8993/$ – see front matter © 2010 Elsevier B.V. All rights reserved.
doi:10.1016/j.brainres.2010.08.090

## 1. Introduction

Rett syndrome (RTT) is a neurodevelopmental disorder that is the leading cause of mental retardation in females (Chahrour and Zoghbi, 2007). Up to 95% of classical RTT cases are caused by mutations in the methyl-CpG-binding protein 2 (MeCP2) gene, which is located at Xq28 (Amir et al., 1999). Knockout mouse models with disrupted MeCP2 function mimic many key clinical features of RTT, including normal early postnatal life followed by developmental regression resulting in motor impairment, irregular breathing and hindlimb clasping (Chen et al., 2001; Guy et al., 2001).

Although MeCP2 was previously thought to function solely as a transcriptional repressor, it was recently shown to act as both a repressor and an activator to regulate the expression of a wide range of genes (Chahrour et al., 2008). This suggests that using only genetic strategies to investigate MeCP2-related biology may be insufficient. Indeed, comparing the transcriptional profiles of whole MeCP2-deficient and wild-type mouse brains revealed subtle and non-specific transcriptional differences. In addition, although several MeCP2 target genes, including brain-derived neurotrophic factor (BDNF) and glial fibrillary acidic protein (GFAP), have been identified, the functional relevance of these genes remains largely unknown (Bienvenu and Chelly, 2006).

One of the most important but unanswered questions is the role of MeCP2 throughout various stages of neural development, particularly at early stages, including the period just prior to and at the onset of neural differentiation. However, the lack of a definitive experimental system has hampered efforts in this direction. Although anatomical studies have demonstrated that the timing of MeCP2 expression in brains is correlated with the maturation of the central nervous system, the fine spatiotemporal pattern of MeCP2 expression during early embryogenesis is largely unknown (Shahbazian et al., 2002). On the other hand, several recent studies that established and/or utilized effective cell culture systems provided valuable information on the roles of MeCP2 in the pathogenesis of RTT (Bienvenu and Chelly, 2006; Chahrour and Zoghbi, 2007). Studies on neural stem cells (NSCs) indicate that MeCP2 may play a role in neuronal maturation (Kishi and Macklis, 2004; Smrt et al., 2007). In another study, MeCP2 was shown to be involved in cell fate determination during neurogenesis (Setoguchi et al., 2006; Tsujimura et al., 2009). Moreover, two studies using an *in vitro* co-culture system have recently reported that MeCP2-deficient astroglia non-cell autonomously affected neuronal dendritic growth (Ballas et al., 2009; Maezawa et al., 2009). Whereas these studies provided important information, the role of MeCP2 throughout neural development is unknown, and in particular, the developmental abnormalities that eventually result in the onset of neurological symptoms in RTT have not yet been elucidated by conventional strategies.

RTT has been reported to be associated with abnormalities in the biogenic amine neurotransmitter/receptor systems, but these findings are controversial due to limitations of the experimental strategies used (Jellinger, 2003; Temudo et al., 2009). Some studies have demonstrated decreases in dopamine levels in the spinal fluid of human RTT patients and/or MeCP2-null animals, however, others have failed to find such changes (Ide et al., 2005; Perry et al., 1988; Samaco et al., 2009; Zoghbi et al., 1989, 1985). Pluripotent embryonic stem (ES) cells show great promise for uncovering the molecular mechanisms of development in various tissues by *in vitro* cell culture. The utility of the ES cell system for addressing a particular problem is largely determined by how efficiently the target cell type can be induced. A recent study described a co-culture system that efficiently induced mouse ES cells to differentiate into dopaminergic neurons (DNs) (Kawasaki et al., 2000). Taken together with both the present status of the controversy concerning dopaminergic abnormalities in RTT and the established experimental system that efficiently induces ES cells towards DNs, DNs may be a good candidate as a target cell type in initial studies that utilize pluripotent ES cells for analyzing functional abnormalities of MeCP2-null neurons.

Here, we develop an MeCP2-null ES cell system for analyzing developmental processes at the cellular level. We examine the role of MeCP2 in maintenance of the undifferentiated ES cell state, neuronal and glial differentiation, DN function, and neuronal maturation. We also show that MeCP2 is involved in the maturation of neurons and gliogenesis.

## 2. Results

### 2.1. *Generation of MeCP2-null ES cells by ACT*

We generated MeCP2-null and control ES cells by ACT as follows: parental ES cells (Me2loxIII6A), in which exons 3 and 4 of the Mecp2 gene on the X chromosome are flanked, were infected by Ad.Cre or control Ad.dE1.3, at a multiplicity of infection of 30 (Takahashi et al., 2006). Subsequently, the infected cells were detached and plated onto a 96-well plates at a very low concentration corresponding to less than one cell per well. Several colonies originating from isolated single cell clones were cultured and expanded in larger dishes. To generate control ES cell lines, the parental ES cells were infected with Ad.dE1.3, instead of Ad.Cre and were handled and expanded in the same way as mutant cells.

The original ES cells were derived from male E14 TG2a cell lines carrying both an X and Y chromosome (Guy et al., 2001). Genomic PCR with primer set 1 (oIMR1436 and oIMR1437) should produce a 400 bp band from hemizygous cells ($Mecp2^{-/y}$) when excision of Mecp2 exon 3 and part of exon 4 occurs, leading to the shortened and amplifiable size of this region (Fig. 1A). Non-excised DNA from parental or control ES cells is too long to be amplified by PCR using primer set 1. Primer set 2 (oIMR 1436 and oIMR 1438) can anneal and amplify only to unexcised DNA in parental or control wild-type ES cells ($Mecp2^{+/y}$) with a predicted band size of 416 bp, but cannot amplify the excised DNA due to the lack of the primer S1438 annealing site (Fig. 1A). The two selected Ad.Cre-infected clones were verified to be hemizygotes ($Mecp2^{-/y}$), in accordance with the results for Mecp2 hemizygous mice (Fig. 1B). In contrast, control ES clones infected by Ad.dE1.3 showed the wild-type band ($Mecp2^{+/y}$), in accordance with the results for wild-type mice (Fig. 1B).

We further confirmed the lack of MeCP2 mRNA expression by RT-PCR of these ES cell clones. Mecp2 has two splice isoforms, Mecp2 e1 and e2 (Kriaucionis and Bird, 2004; Mnatzakanian et al., 2004). The Ad.dE1.3-infected control ES

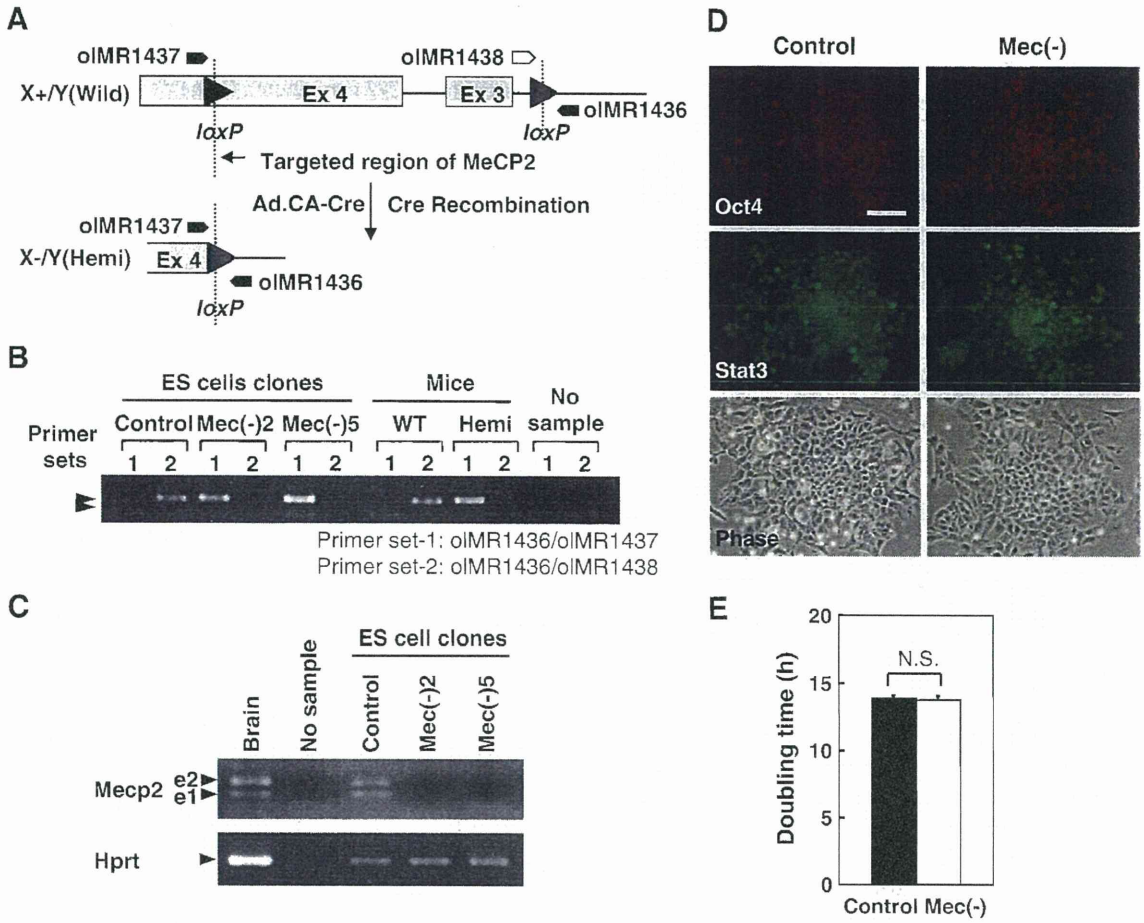


**Fig. 1 – Generation and phenotypic analysis of MeCP2-null ES cells. (A) Targeted mutation of the Mecp2 locus. (B) Genotyping of control (Mecp2$^{+/y}$) and two MeCP2-null (Mecp2$^{-/y}$; Mec(–)) ES cell clones, and of MeCP2 wild-type and hemizygous mice was performed by PCR. Primer set 1 (oIMR 1437 and oIMR 1436) amplifies a ~400 bp mutant band, whereas primer set 2 (oIMR1438 and oIMR 1436) amplifies a 416 bp wild-type band. (C) mRNA expression of Mecp2 e1 and e2 variants in a control and two MeCP2-null ES cell clones was analyzed by RT-PCR. Wild-type mouse brain was used as a positive control. (D) The control and the MeCP2-null ES cells were stained with anti-Oct4 or anti-STAT3 antibody. Scale bar=80 μm. (E) Doubling times of undifferentiated control and MeCP2-null ES cells are shown. N.S., no significant difference (control versus MeCP2-null ES cells, n=19 each).**

cells showed expression of both Mecp2 splice variants, e1 and e2, whereas neither Mecp2 variant was detectable in both Ad. Cre-infected MeCP2-null ES cell clones (Fig. 1C). Thus, two MeCP2-null (Mecp2$^{-/y}$) and one control (Mecp2$^{+/y}$) ES cell clones were efficiently generated. In the following experiments, we use one of two MeCP2-null ES cell lines (clone 2) and one control ES cell line.

### 2.2. *Loss of MeCP2 does not appear to affect undifferentiated ES cells*

We first examined whether MeCP2 is required in undifferentiated ES cells. Prominent expression of Oct4 and Stat3, markers of the undifferentiated state, was found in the nuclei of almost all cells in both MeCP2-null and control ES cells by immunostaining (Fig. 1D). No differences in undifferentiated growth were observed between the two (Fig. 1E). Thus, MeCP2 does not appear to be critical for maintaining the undifferentiated state or for ES cell growth.

### 2.3. *MeCP2 is not involved in the efficiency of neural differentiation*

RT-PCR analysis showed that both Mecp2 variants, e1 and e2, were expressed in control ES cells in the undifferentiated state, as well as throughout all developmental stages (Fig. 2A).

We examined the role of MeCP2 in neuronal differentiation by comparing the phenotypes of control and MeCP2-null ES cells during differentiation. Neither the number nor the morphology of the differentiating ES colonies was significantly different between the two groups, suggesting that MeCP2 is not essential for cell growth during neural differentiation (Fig. 2B and C).

We next examined whether MeCP2 affected neuronal differentiation by immunostaining for Nestin, β-Tubulin type III (TuJ), and Tyrosine hydroxylase (TH), markers for early neuronal cells (including NSCs), differentiated neurons, and DNs, respectively (Fig. 3A–C). The percentage of Nestin-, TuJ-, and TH-positive colonies reached a maximum on day

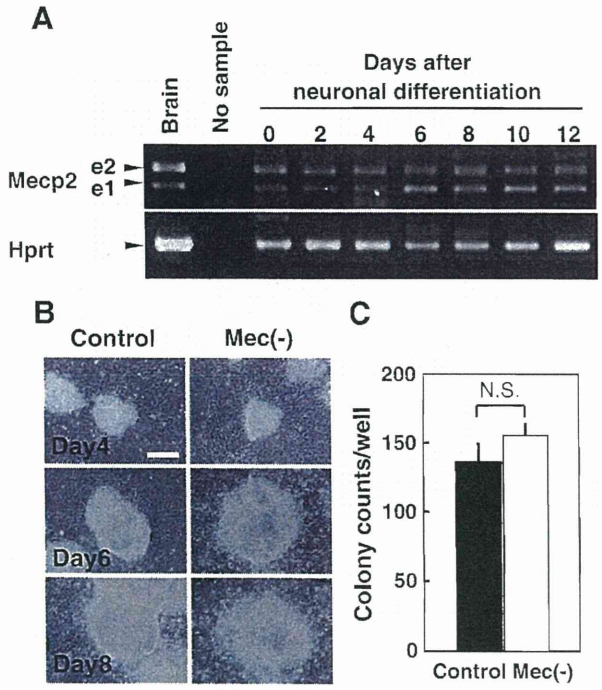


**Fig. 2 – Neural differentiation of MeCP2-null ES cells. (A) mRNA expression of Mecp2 e1 and e2 variants in control ES cells on the indicated days after the start of co-culture on PA6 cells was analyzed by semi-quantitative RT-PCR. Wild-type mouse brain was used as a positive control. (B) Representative images of control and MeCP2-null ES cell colonies on the indicated days after co-culture on PA6 cells. Scale bar=200 μm. (C) The number of colonies per well was counted on day 10.**

8 and did not differ between the two groups. Thus, loss of MeCP2 does not affect the efficiency of neuronal differentiation. The percentage of Nestin-, TuJ-, and TH-positive MeCP2-null colonies was higher than that of control colonies on day 4, and the percentage of Nestin-positive MeCP2-null colonies on day 12 was lower than that of the controls, although the slightly precocious differentiation was not significant. The results suggest that MeCP2 is not essential for induction of neuronal differentiation, at least induction toward DNs.

### 2.4. *Loss of MeCP2 causes immature resting and active membrane properties in ES cell-derived neurons*

To analyze neuronal maturity, the membrane properties of control and MeCP2-null ES cell-derived neurons were examined by electrophysiology on days 10–12 (Table 1). The peak current densities of the voltage-dependent $Na^+$ currents ($I_{Na}$s) underlying the rising phase of the action potential and the A-type $K^+$ currents ($I_A$s) were significantly smaller in the MeCP2-null ES cell-derived neurons than in the controls (Fig. 4A and B). In contrast, the peak currents of the delayed rectifier $K^+$ currents ($I_{DR}$s) did not significantly differ between the control and MeCP2-null ES cell-derived neurons (Fig. 4C). In addition, the repetitive spikes showed a relatively high firing frequency and rundown in amplitude in the MeCP2-null ES cell-derived neurons (Fig. 4D). The rundown may be due to a decrease in expression of $I_{Na}$s and the $I_A$s. These results suggest that MeCP2 contributes to the development of resting and active membrane properties, and that MeCP2-null ES cell-derived neurons do not reach maturity.

### 2.5. *MeCP2 does not appear to affect dopaminergic function*

To examine the involvement of MeCP2 in DN function, dopamine production and release were investigated by reverse phase HPLC in MeCP2-null and control ES cell-derived neurons on day 10 of culture. In response to a depolarizing stimulus, DNs derived from MeCP2-null ES cells released as much dopamine into the medium as did control cells (Fig. 5). Thus, MeCP2 is not critical for the dopaminergic function of DNs, at least in this experimental system.

### 2.6. *MeCP2 deficiency accelerates glial differentiation*

Because interactions between neurons and glia are essential for the development and function of neurons (Corbin et al., 2008; Stevens, 2008), we examined changes in expression of the glial marker GFAP in ES colonies during neural differentiation. GFAP-positive colonies emerged earlier and were present at a higher percentage on days 8 and 12 in MeCP2-null ES cells compared to controls (Fig. 6A and B), consistent with the GFAP expression observed in colonies (Fig. 6C). The significantly accelerated glial differentiation in MeCP2-deficient cells suggests that MeCP2 negatively regulates glial differentiation. In addition, the timing of differentiation, with the start of neuronal differentiation preceding the start of glial differentiation, as well as the presence of both neurons and glia in differentiated ES colonies mirror normal neural development (Qian et al., 2000; Stevens, 2008), underscore the usefulness of this experimental system.

## 3. Discussion

The overall role of MeCP2 throughout neural development, particularly at early stages before the onset of neural differentiation, has not been investigated due to the lack of a definitive experimental system or materials. In this study, we first demonstrated that MeCP2-null ES cell could be feasibly generated by applying the *in vitro* ACT method to loxP-floxed ES cells that were originally engineered for a generation of conditional knockout mouse (Takahashi et al., 2006). Just as there were no significant adverse effects from ACT on cell cycle regulation, cell viability, or the efficiency of differentiation in ES cells, the MeCP2-null and the control ES cells generated by ACT worked with no problems in several types of experiments in the previous and the present study (Takahashi et al., 2006). In addition, the co-culture method that was used in the present study has the advantages of both technical feasibility and high efficiency of dopaminergic differentiation (Kawasaki et al., 2000). Our experimental system of comparing MeCP2-null and control ES cells throughout their developmental stages, including in the undifferentiated state and at the early stage of neural development, provided important information about the role of MeCP2 in neural development.

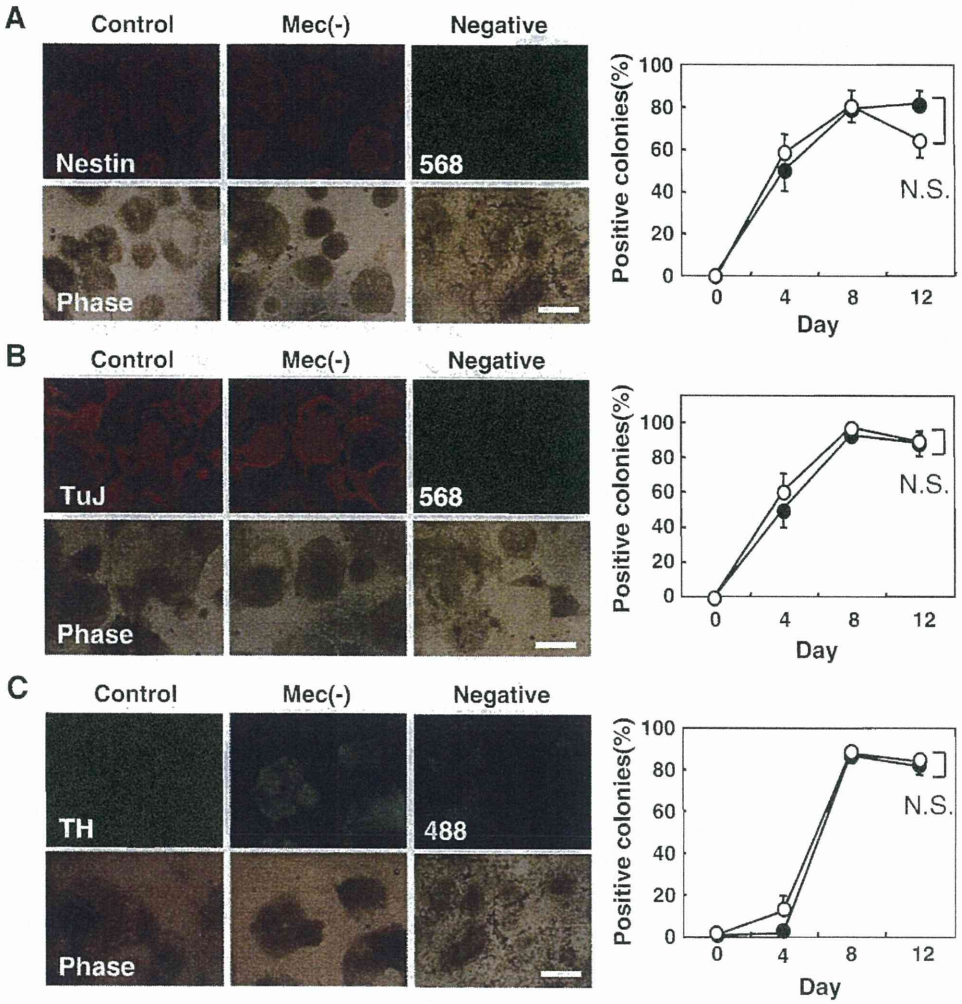


**Fig. 3 – Neuronal differentiation of MeCP2-null ES cells. (A–C) Control (closed circle) and MeCP2-null (open circle) ES cells on days 4, 8, and 12 were stained with antibody against Nestin (A), TuJ (B), or TH (C). Negative control indicates colonies on day 12 that were stained with only the secondary Alexa Fluor 488 or 568 antibodies without primary antibodies. N.S., no significant difference (control versus MeCP2-null ES cells at each time point). Between 50 and 200 colonies per well were counted to calculate the mean±SD (Nestin; $n=5$, TuJ; $n=5$, and TH; $n=3$) and the results were verified in three different experiments. Representative images from day 12 are shown on the left. Scale bar=0.5 mm.**

Using this system, we have clarified several important issues, some of which are consistent with previous findings. First, we demonstrated that MeCP2 is not essential for the maintenance or growth of undifferentiated ES cells, supporting the previous finding that absence of MeCP2 did not cause embryonic lethality in mice (Guy et al., 2001). Second, MeCP2 deficiency has a minimal effect on neurogenesis, consistent with the fact that the brains of RTT patients and MeCP2-null mice are morphologically and phenotypically normal at birth (Armstrong, 2002; Chahrour and Zoghbi, 2007). Thus, MeCP2 is likely not an essential part of the machinery that advances neurogenesis. On the other hand, while it has been reported that MeCP2 was involved in neuronal maturation rather than cell fate decisions (Kishi and Macklis, 2004; Smrt et al., 2007), the present results suggested that MeCP2 was remarkably somewhat involved in negative regulation of glial differentiation and neuronal maturation. Apparently inconsistent results between the previous and present studies may be due to the difference in experimental systems. For instance, MeCP2 was expressed in neurons and undifferentiated neuroepithelial cells at high and almost undetectable levels, respectively, in the experimental system of the previous study (Kishi and Macklis, 2004), whereas in the present system MeCP2 expressions were clearly detected in not only ES cell-derived differentiated neurons but also in undifferentiated ES cells. This aspect of the present experimental system may have the advantage of being able to sensitively and carefully detect any possible phenotypes in order to determine whether MeCP2 affects neural development, including gliogenesis, during any stage, including early stages before the onset of neural differentiation.

In contrast, MeCP2-null ES-derived neurons are electrophysiologically immature, suggesting that MeCP2 contributes to the development of the active membrane properties. Biella et al. have reported that voltage-gated $Na^+$ currents gradually increase during neuronal maturation, but that $I_{DR}$s is already

**Table 1 – Differences in electrophysiological parameters between control and MeCP2-null ES-derived cells.**

| | Parameters | Control | Mec(–) |
|---|---|---|---|
| $I_{Na}$ | Peak amplitude, pA | −1060±140(4) | −701.8±184.9(5)* |
| | Current density, pA/pF | −96.4±6.5(4) | −64.2±8.7(5)* |
| $I_A$ | Peak amplitude, pA | 89.0±32.2(4) | 30.1±8.4(4)* |
| | Current density, pA/pF | 8.3±1.7(4) | 3.0±0.7(4)* |
| $I_{DR}$ | Peak amplitude, pA | 169.2±87.1(3) | 105.7±53.4(4) |
| | Current density, pA/pF | 15.8±7.2(3) | 11.0±7.2(4) |
| | Membrane capacitance, pF | 10.7±1.6(11) | 10.3±1.8(13) |
| | $V_{Rm}$, mV | −52.8±11.4(6) | −52.1±10.7(7) |
| | Threshold, mV | −44.4±4.9(6) | −37.6±1.0(6)* |
| | Firing frequency, Hz | 5.8±1.0(6) | 9.3±0.8(6)* |

$I_{Na}$; voltage-dependent $Na^+$ current, $I_A$; A-type $K^+$ current, $I_{DR}$; delayed rectifier $K^+$ current, $V_{Rm}$; resting membrane potential
Numbers in parentheses indicate the recording cell number.
Firing frequency is derived from mean firing rate during the injection of depolarizing current of which amplitude is two times of the threshold.
* Indicates statistical significance between the control and the MeCP2-null ES-derived neurons by Student's test with $p<0.05$.

at a mature state at early stages of neural development in ES-derived NSCs (Biella et al., 2007). The amplitude of $I_A$s also increases during the late embryonic-early postnatal developmental period in hippocampal neurons (Ficker and Heinemann, 1992). Thus, MeCP2 may be required for neuronal maturation (development of voltage-gated $Na^+$ currents and $I_A$s), suggesting that some neuronal symptoms in RTT may be caused by immature neuronal membrane properties.

In terms of the neural immaturity in MeCP2-deficient cultures, it should be noted that loss of MeCP2 led to drastically increased gliogenesis. The involvement of MeCP2 in gliogenesis may be supported by previous studies, although their data were indirect and limited to middle and late phases of neural development (Deguchi et al., 2000; Nagai et al., 2005; Setoguchi et al., 2006). For instance, inhibition of MeCP2 in E18 non-neuronal mouse cells inhibited cell growth (Nagai et al., 2005), and ectopic overexpression of MeCP2 inhibited E14.5 neuroepithelial cells from differentiating into GFAP-positive cells (Setoguchi et al., 2006). Moreover, MeCP2 binds to a highly methylated region in the GFAP promoter. Thus, the authors suggested that MeCP2 is involved in restricting differentiation

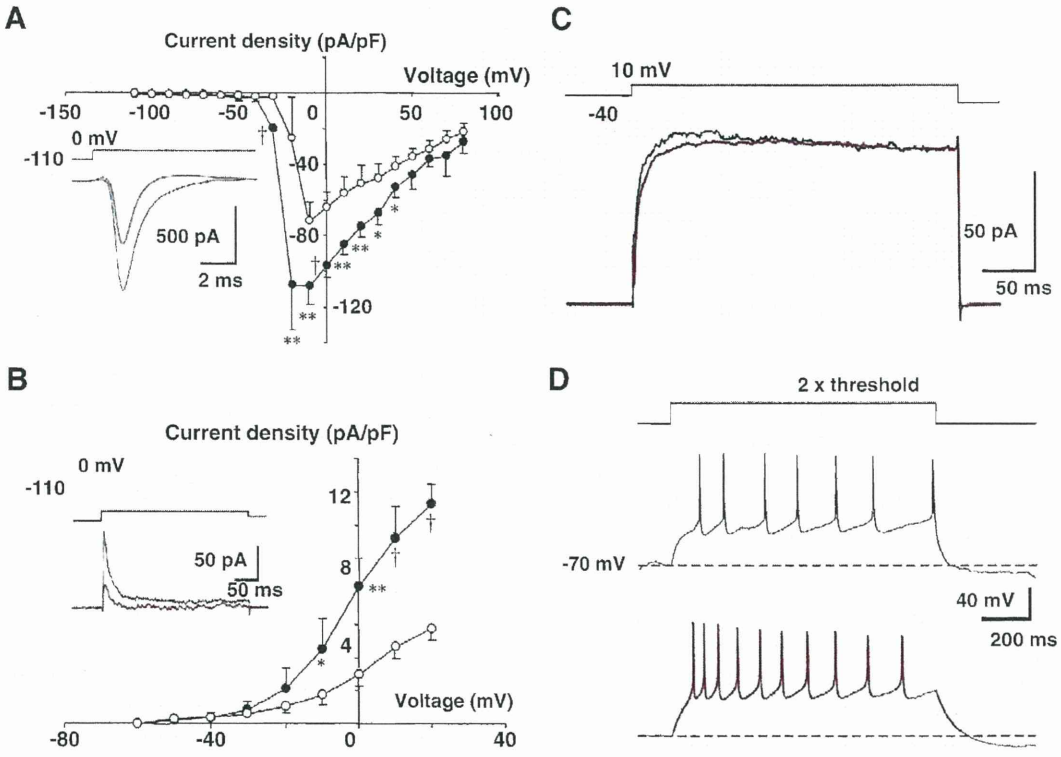


**Fig. 4 – Electrophysiological analysis of control and MeCP2-null ES cell-derived neurons. (A) Voltage-dependent $Na^+$ currents ($I_{Na}$s) were recorded from control and MeCP2-null ES cell-derived neurons on days 10–12. Current density–voltage (*I*–*V*) relationships were obtained from control ($n=4$, closed circles) and MeCP2-null neurons ($n=5$, open circles). Inset traces show the mean $I_{Na}$s elicited by the voltage step pulse from −110 to 0 mV in control (black, $n=4$) and MeCP2-null neurons (red, $n=5$). Symbols for statistical significance: *$P<0.05$; **, $P<0.01$; and †$P<0.001$ (control versus MeCP2-null neurons). (B) Fast inactivating $K^+$ currents ($I_A$s) were recorded from control and MeCP2-null neurons. *I*–*V* relationships were obtained from control ($n=4$, closed circles) and MeCP2-null neurons ($n=4$, open circles). Inset traces show the mean $I_A$s elicited by the voltage step pulse from −110 to 0 mV. (C) Sustained $K^+$ currents ($I_{DR}$s) were recorded from control (black, $n=3$) and MeCP2-null neurons (red, $n=4$). Each trace shows the mean $I_{DR}$s elicited by the voltage step pulse from −40 to +10 mV. (D) Response to the depolarizing current pulse injection of membrane was recorded from control (black, $n=6$) and MeCP2-null neurons (red, $n=6$). In each trace, the dashed line indicates the holding membrane potential (−70 mV), and upward deflections during the current pulse injection indicate $Na^+$ spikes.**

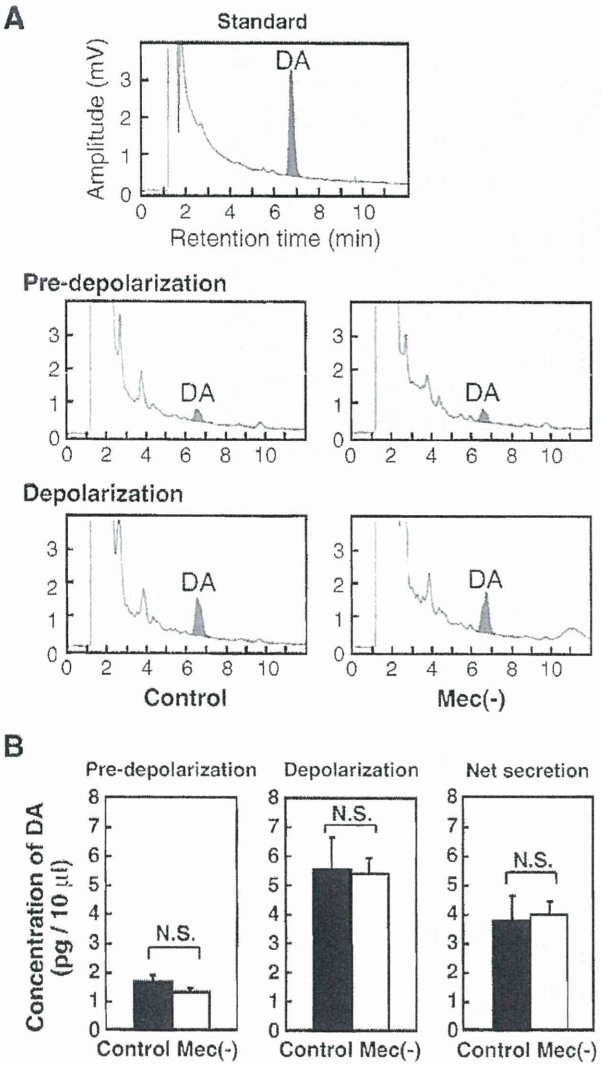


**Fig. 5 – Dopamine production and release in MeCP2-null ES cell-derived DNs. (A) Dopamine releases in the media of control and MeCP2-null ES cells on day 10 were analyzed by reverse phase HPLC. The standard panel shows chromatography of a standard solution. DA indicates peaks of dopamine. The retention time for dopamine was 6.5 min in each case. (B) The graphs represent the quantitative HPLC data for dopamine secretion. Dopamine secretion was measured in samples incubated for 15 min with HBSS (pre-depolarization) or high $K^+$ HBSS (depolarization). Pre-depolarization indicates the spontaneous secretion of dopamine. Net secretion is the depolarized peak release minus the spontaneous dopamine release and shows the response in the presence of potassium. N.S., no significant difference (control versus MeCP2-null ES cells, $n=8$ each).**

plasticity in neurons, possibly by stage-specific and neuron-specific methylation of glial genes (Setoguchi et al., 2006).

Interestingly, brain magnetic resonance in MeCP2-null mice demonstrated that metabolism in both neurons and glia was affected (Saywell et al., 2006). In addition, a study using *in vitro* co-culture system has recently demonstrated that MeCP2 mutant astrocytes and their conditioned medium failed to support normal dendritic morphology of hippocampal neurons, suggesting that MeCP2-deficient astrocytes have a non-cell autonomous effect on neuronal properties (Ballas et al., 2009; Maezawa et al., 2009). In general, the coordinated interactions between glia and neurons are crucial for normal neuronal development and function (Allen and Barres, 2009; Corbin et al., 2008; Stevens, 2008). Together with previous data, our results suggest that the main physiological role of MeCP2 in neural development is the inhibition of gliogenesis, and that distorted interactions with abnormally developed glia result in electrophysiologically immature neurons.

Finally, this study may at least in part resolve some of the controversy over whether or not abnormalities in biogenic amine neurotransmitter/receptor systems are associated with RTT (Matsuishi et al., 2001; Temudo et al., 2009; Wenk, 1995). Discrepancies between different studies may be due to the limitations of the experimental strategies, which involved clinical examination of dopamine levels in central spinal fluid, dopamine D2 receptors, or pathological alterations in symptomatic RTT patients (Chiron et al., 1993; Lekman et al., 1990; Perry et al., 1988; Zoghbi et al., 1989, 1985). Here, we demonstrate that MeCP2 is involved in neither the differentiation nor the dopamine production and release of DNs. This has important clinical implications, since whatever abnormalities might exist in the dopaminergic system in RTT patients, they are not directly related to defects in the DNs themselves. However, a potential limitation of the present study is that the ES cell-derived DNs might not be entirely equivalent to DNs in adolescent RTT patients, even though almost all the ES cell colonies were TH-positive. Using this experimental system to uncover the cellular and molecular characteristics of MeCP2-null DNs, in conjunction with studies of MeCP2-null mice and clinical examination of RTT patients, will answer this question definitively in the future.

In conclusion, we have developed an *in vitro* system for analyzing neuronal development and the function of MeCP2. We found that MeCP2 is not essential for maintaining the undifferentiated ES cell state, for neurogenesis, or for DN function; rather, it is mainly involved in inhibiting gliogenesis. Imperfect neuronal maturity, probably resulting from abnormal gliogenesis, may be involved in the pathogenesis of RTT. All the information is useful not only for understanding the developmental roles of MeCP2 and the pathogenesis of RTT, but also for developing therapeutic strategies for RTT in the future.

## 4. Experimental procedures

### 4.1. *Recombinant adenoviral vectors*

E1-deleted, replication-deficient adenoviral vector expressing Cre under the transcriptional control of the cytomegalovirus early enhancer and chicken beta-actin promoter (Ad.Cre) or no gene (Ad.dE1.3) was prepared as described previously (Chen et al., 1995; Takahashi et al., 2006).

### 4.2. *ES cell culture and ACT*

Mouse ES cells in which exons 3 and 4 of Mecp2 were flanked by loxP sites, and which were previously used to generate

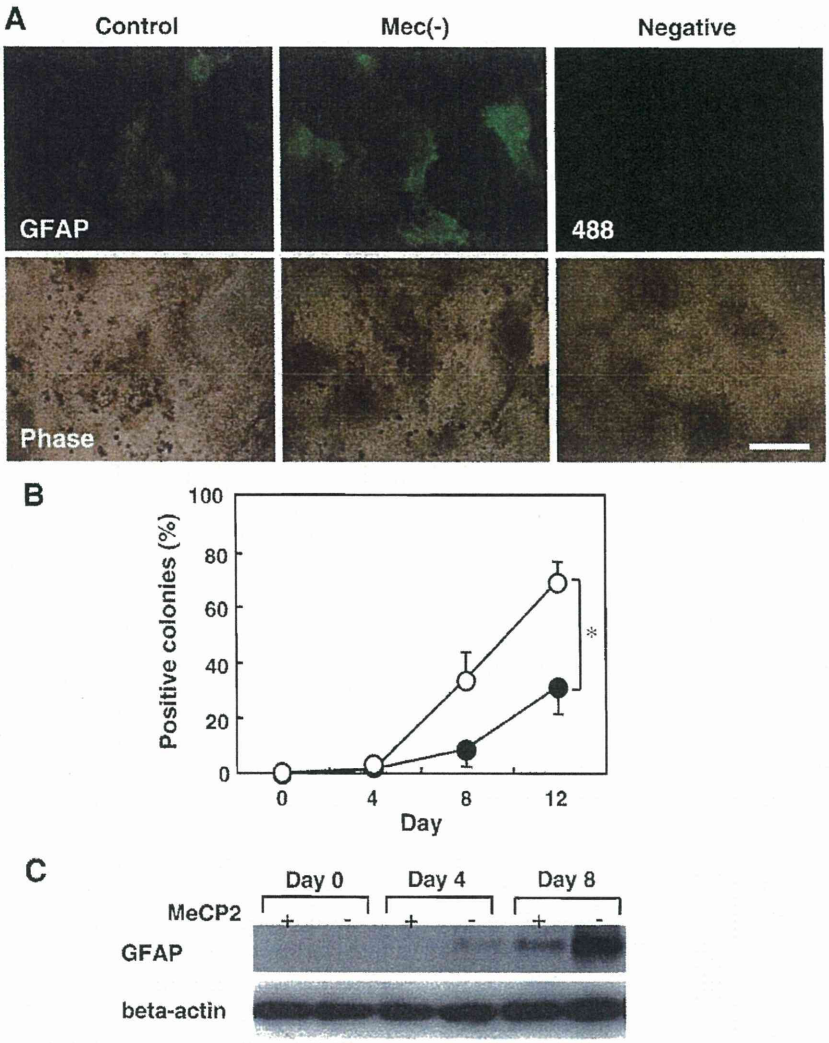


**Fig. 6 – Glial differentiation of MeCP2-null ES cells. Control or MeCP2-null ES cell colonies 4, 8, and 12 days after co-culture on PA6 cells were immunostained for GFAP. (A) The top and bottom pictures show immunofluorescent microscopic and phase-contrast observations of ES colonies, respectively, which were stained with an anti-GFAP (green) antibody on day 12. Negative control images show colonies stained with the secondary Alexa Fluor 488 antibody on day 12. Scale bar = 0.5 mm. (B) The graph shows the percentage of control (closed circle) and MeCP2-null (open circle) GFAP-positive ES cell colonies on the indicated days. *$P < 0.05$ (control versus MeCP2-null ES cells, $n = 5$ each, 50–200 colonies per well). Data are means ± SD for three separate measurements from different experiments. (C) Expressions of GFAP protein in control and MeCP2-null ES cells on the indicated days were analyzed by Western blot. Beta-actin protein levels were analyzed in the same way as an internal control.**

MeCP2-null mice, were provided by Dr. A. Bird (Guy et al., 2001). ES cells were maintained in the undifferentiated state without feeder cells on gelatin-coated dishes in Glasgow Minimum Essential Medium (G-MEM, GIBCO/BRL, Grand Island, NY, USA) supplemented with 10% fetal bovine serum (FBS), 2 mM L-glutamine (GIBCO/BRL), 1 mM pyruvate (GIBCO/BRL), 0.05 mM 2-mercaptoethanol (2-ME, Nacalai Tesque, Inc., Kyoto, Japan), 0.1 mM nonessential amino acids (GIBCO/BRL), and 2000 U/ml leukemia inhibitory factor (ESGRO, Chemicon International, Temecula, CA) as previously described (Guy et al., 2001; Kawai et al., 2004; Takahashi et al., 2006). MeCP2-null and control ES cells were generated by the ACT method using Ad.Cre and Ad.dE1.3, respectively (Chen et al., 1995; Takahashi et al., 2006). Details are described in the Results section.

Doperminergic neurons were induced essentially as previously described, with some modifications (Kawasaki et al., 2000; Takahashi et al., 2006). Briefly, 1000 MeCP2-null or control ES cells were placed on feeder PA6 cells that had been seeded on collagen-coated eight-well glass plates. Subsequently, these ES cells were co-cultured with PA6 cells in differentiation medium, which consists of G-MEM supplemented 10% knockout serum replacement (KSR, GIBCO/BRL), 2 mM L-glutamine, 1 mM pyruvate, 0.1 mM nonessential amino acids, and 0.1 mM 2-mercaptoethanol as described previously (Kawasaki et al., 2000). The differentiation medium was changed on day 4 and every other day thereafter. After 8 days in differentiation medium, cells were cultured in G-MEM supplemented with N2 (GIBCO/BRL), 100 mM

tetrahydrobiopterin, 200 mM ascorbate, 1 mM pyruvate, 0.1 mM nonessential amino acids, and 0.1 mM 2-mercaptoethanol.

### 4.3. Animals

The tails of MeCP2-null mice were used as positive controls for genomic PCR (Fig. 1B) in accordance with a protocol approved by the Animal Research Committee of Kurume University and the National Institutes of Health Guidelines for the Care and Use of Laboratory Animals.

### 4.4. PCR analysis

Genomic DNA was extracted from ES cells and PCR genotyping was performed on genomic DNA using oIMR1436, oIMR1437, and oIMR1438 primers and the protocol provided by the manufacturer (http://jaxmice.jax.org/pub-cgi/protocols/protocols.sh?objtype=protocol&protocol_id=598) (Fig. 1A) (Guy et al., 2001).

Extraction of total RNA, RT-PCR analysis, and electrophoresis were carried out as described previously (Kawai et al., 2004; Takahashi et al., 2006). PCR conditions were as follows: 40 cycles of 94 °C for 30 s, 61 °C for 60 s, and 74 °C for 60 s, using the mouse Mecp2 exon-specific primers 5′-GGTAAAACCGGTCGG GAAAATG-3′ (sense) and 5′-TTCAGTGGCTTGTCTCTGAG-3′ (antisense) (Kriaucionis and Bird, 2004).

### 4.5. Immunocytochemistry

Cells were stained using antibodies against Nestin (dilution 1:100, clone 25, BD Biosciences Pharmingen, San Diego, CA), Tyrosine hydroxylase (TH) (dilution 1:100, clone AB152, Chemicon International), β-Tubulin type III (dilution 1:500, TuJ, Sigma-Aldrich, Inc., St. Louis, MO), GFAP (dilution 1:500, clone G-A-5, Sigma-Aldrich, Inc.), Oct-4 (dilution 1:500, clone C-10, Santa Cruz Biotechnology, Inc., Santa Cruz, CA), or Stat-3 (dilution 1:500, C-20, Santa Cruz Biotechnology, Inc.), together with secondary fluorescent antibodies (dilution 1:500) as described previously (Kawai et al., 2004; Takahashi et al., 2006). As a negative control, cells were stained with only secondary fluorescent antibodies without primary antibodies (Figs. 3, 6A, and Suppl. Fig. 1).

### 4.6. Immunoblotting

Protein was extracted from ES cells and Western blot analysis was performed using anti-GFAP (clone G-A-5) and anti-Actin (clone AC-40, Sigma-Aldrich, Inc.) monoclonal antibodies, and detected with horseradish peroxidase-conjugated anti-mouse IgG (DakoCytomation, Glostrup, Denmark) and chemiluminescent substrate (Chemi-Lumi One, Nacalai Tesque, Inc.), as described previously (Takahashi et al., 2006).

### 4.7. Electrophysiological analysis

Electrophysiological measurements were performed as described previously (Murai and Akaike, 2005). Briefly, whole cell patch-clamp recordings were made from 29 ES cell-derived neurons with glass patch-pipettes. The resistance of patch electrodes was 4–8 MΩ. Cells were voltage or current clamped. The membrane currents or potentials were measured with a patch-clamp amplifier (Axopatch 200A, Axon Instruments Inc., Union City, CA, USA). Whole cell currents or membrane potentials were low-pass filtered at 1–2 kHz, digitized at a sampling rate of 20 kHz, and stored on a computer hard disc (pCLAMP 8, Axon Instruments Inc.). Series resistance was compensated by 50–70%. All experiments were performed at room temperature (21–24 °C).

The membrane was first held at −110 mV and then depolarized by voltage step pulses (300 ms duration) from −110 to +80 mV with 10 mV steps to elicit the membrane currents. In the absence and presence of voltage-dependent $Na^+$ channel blocker, tetrodotoxin (TTX, 300 nM), the total membrane currents and TTX resistant (TTX-R) currents were obtained, respectively. The voltage-dependent sodium ($Na^+$) current, which is TTX sensitive (TTX-S), was obtained by subtracting the TTX-R currents from the total membrane currents in both the control and MeCP2-null ES cell-derived neurons.

Two types of voltage-dependent potassium ($K^+$) currents were also recorded in both the control and the MeCP2-null ES cell-derived neurons: fast inactivating $K^+$ current (A-type $K^+$ current, $I_A$) and sustained $K^+$ current (delayed rectifier $K^+$ current, $I_{DR}$), sensitive to 4-aminopyridine (4-AP, 1 mM) and tetraethylammonium-chloride (TEA-Cl, 20 mM), respectively. The voltage step pulse from −110 to +20 mV with 10 mV step (300 ms duration) in the presence of TTX (300 nM) elicited the combined membrane $K^+$ currents. To obtain $I_{DR}$, the membrane was first held at −40 mV and then depolarized from −40 to +20 mV with 10 mV steps (300 ms duration), because $I_A$ inactivated at −40 mV and $I_{DR}$ was activated from −40 mV. Subtraction of $I_{DR}$ from the combined membrane $K^+$ currents yielded $I_A$.

In current-clamp recording, injection of the depolarizing current pulse (2 ms, 0.15–0.20 nA) elicited an action potential just after the end of the current injection. In both control and MeCP2-null ES cell-derived neurons, injection of a prolonged depolarizing current pulse (1 s duration and two times the intensity for the threshold) elicited repetitive firings during membrane depolarization.

### 4.8. High performance liquid chromatography (HPLC)

To measure dopamine content and secretion in MeCP2-null and control ES cells that were differentiated into DNs on PA6 cells for 10 days, an HPLC electrochemical detector (ECD) system (HTEC-500, Eicom Corp., Kyoto, Japan) was used in accordance with the manufacturer's protocol, with some modifications (Kawasaki et al., 2000). Briefly, ES cells cultured in six-well plates were washed twice with Hanks' balanced salt solution (HBSS), then incubated for 15 min in high $K^+$ (56 mM) HBSS to evoke membrane depolarization. The incubation buffer (a 500 ml aliquot) was collected and centrifuged at 800×*g* for 10 min to remove detached cells, and the 400 ml supernatant was mixed with 400 ml of 20 mM hydrochloric acid and 100 mM EDTA. Ten microliters of each sample was injected into the HPLC-ECD system and separated with a reverse phase column (Eicompak CA-50DS, Eicom) using 0.1 M phosphate buffer (pH 6.0) containing 2.3 mM 1-octanesulfonic acid, 0.13 mM EDTA, and 20% methanol as a

mobile phase at a flow rate of 0.23 ml/min. The retention time for dopamine was 6–8 min. The amount of dopamine in each sample was calculated by using the peak height ratio relative to the standard dopamine hydrochloride (H8502, Sigma-Aldrich, Inc.) solution.

### 4.9. *Statistical analysis*

Quantitative results are expressed as means±SD. The Student's t-test was used to compare data, with $p<0.05$ considered significant.

Supplementary materials related to this article can be found online at doi:10.1016/j.brainres.2010.08.090.

## Competing interests statement

The authors declare that they have no competing financial interests.

## Acknowledgments

This work was supported in part by a project for establishing open research centers in private universities, a Grant-in-Aid for Scientific Research (B) and a Grant-in-Aid for Young Scientists (B) from the Japan Society for the Promotion of Science, and by a Grant from Terumo Life Science Foundation. We would like to thank Adrian Bird for providing the MeCP2 targeted ES cells; and Kaori Noguchi, Chikako Goto, and Aya Niihara for technical assistance.

## REFERENCES

Allen, N.J., Barres, B.A., 2009. Neuroscience: Glia—more than just brain glue. Nature 457, 675–677.

Amir, R.E., Van den Veyver, I.B., Wan, M., Tran, C.Q., Francke, U., Zoghbi, H.Y., 1999. Rett syndrome is caused by mutations in X-linked MECP2, encoding methyl-CpG-binding protein 2. Nat. Genet. 23, 185–188.

Armstrong, D.D., 2002. Neuropathology of Rett syndrome. Ment. Retard. Dev. Disabil. Res. Rev. 8, 72–76.

Ballas, N., Lioy, D.T., Grunseich, C., Mandel, G., 2009. Non-cell autonomous influence of MeCP2-deficient glia on neuronal dendritic morphology. Nat. Neurosci. 12, 311–317.

Biella, G., Di Febo, F., Goffredo, D., Moiana, A., Taglietti, V., Conti, L., Cattaneo, E., Toselli, M., 2007. Differentiating embryonic stem-derived neural stem cells show a maturation-dependent pattern of voltage-gated sodium current expression and graded action potentials. Neuroscience 149, 38–52.

Bienvenu, T., Chelly, J., 2006. Molecular genetics of Rett syndrome: when DNA methylation goes unrecognized. Nat. Rev. Genet. 7, 415–426.

Chahrour, M., Zoghbi, H.Y., 2007. The story of Rett syndrome: from clinic to neurobiology. Neuron 56, 422–437.

Chahrour, M., Jung, S.Y., Shaw, C., Zhou, X., Wong, S.T., Qin, J., Zoghbi, H.Y., 2008. MeCP2, a key contributor to neurological disease, activates and represses transcription. Science 320, 1224–1229.

Chen, R.Z., Akbarian, S., Tudor, M., Jaenisch, R., 2001. Deficiency of methyl-CpG binding protein-2 in CNS neurons results in a Rett-like phenotype in mice. Nat. Genet. 27, 327–331.

Chen, S.H., Chen, X.H., Wang, Y., Kosai, K., Finegold, M.J., Rich, S.S., Woo, S.L., 1995. Combination gene therapy for liver metastasis of colon carcinoma in vivo. Proc. Natl. Acad. Sci. U. S. A. 92, 2577–2581.

Chiron, C., Bulteau, C., Loc'h, C., Raynaud, C., Garreau, B., Syrota, A., Maziere, B., 1993. Dopaminergic D2 receptor SPECT imaging in Rett syndrome: increase of specific binding in striatum. J. Nucl. Med. 34, 1717–1721.

Corbin, J.G., Gaiano, N., Juliano, S.L., Poluch, S., Stancik, E., Haydar, T.F., 2008. Regulation of neural progenitor cell development in the nervous system. J. Neurochem. 106, 2272–2287.

Deguchi, K., Antalffy, B.A., Twohill, L.J., Chakraborty, S., Glaze, D.G., Armstrong, D.D., 2000. Substance P immunoreactivity in Rett syndrome. Pediatr. Neurol. 22, 259–266.

Ficker, E., Heinemann, U., 1992. Slow and fast transient potassium currents in cultured rat hippocampal cells. J. Physiol. 445, 431–455.

Guy, J., Hendrich, B., Holmes, M., Martin, J.E., Bird, A., 2001. A mouse Mecp2-null mutation causes neurological symptoms that mimic Rett syndrome. Nat. Genet. 27, 322–326.

Ide, S., Itoh, M., Goto, Y., 2005. Defect in normal developmental increase of the brain biogenic amine concentrations in the mecp2-null mouse. Neurosci. Lett. 386, 14–17.

Jellinger, K.A., 2003. Rett syndrome—an update. J. Neural Transm. 110, 681–701.

Kawai, T., Takahashi, T., Esaki, M., Ushikoshi, H., Nagano, S., Fujiwara, H., Kosai, K., 2004. Efficient cardiomyogenic differentiation of embryonic stem cell by fibroblast growth factor 2 and bone morphogenetic protein 2. Circ. J. 68, 691–702.

Kawasaki, H., Mizuseki, K., Nishikawa, S., Kaneko, S., Kuwana, Y., Nakanishi, S., Nishikawa, S.I., Sasai, Y., 2000. Induction of midbrain dopaminergic neurons from ES cells by stromal cell-derived inducing activity. Neuron 28, 31–40.

Kishi, N., Macklis, J.D., 2004. MECP2 is progressively expressed in post-migratory neurons and is involved in neuronal maturation rather than cell fate decisions. Mol. Cell. Neurosci. 27, 306–321.

Kriaucionis, S., Bird, A., 2004. The major form of MeCP2 has a novel N-terminus generated by alternative splicing. Nucleic Acids Res. 32, 1818–1823.

Lekman, A., Witt-Engerstrom, I., Holmberg, B., Percy, A., Svennerholm, L., Hagberg, B., 1990. CSF and urine biogenic amine metabolites in Rett syndrome. Clin. Genet. 37, 173–178.

Maezawa, I., Swanberg, S., Harvey, D., LaSalle, J.M., Jin, L.W., 2009. Rett syndrome astrocytes are abnormal and spread MeCP2 deficiency through gap junctions. J. Neurosci. 29, 5051–5061.

Matsuishi, T., Yamashita, Y., Kusaga, A., 2001. Neurobiology and neurochemistry of Rett syndrome. Brain Dev. 23 (Suppl 1), S58–S61.

Mnatzakanian, G.N., Lohi, H., Munteanu, I., Alfred, S.E., Yamada, T., MacLeod, P.J., Jones, J.R., Scherer, S.W., Schanen, N.C., Friez, M.J., Vincent, J.B., Minassian, B.A., 2004. A previously unidentified MECP2 open reading frame defines a new protein isoform relevant to Rett syndrome. Nat. Genet. 36, 339–341.

Murai, Y., Akaike, T., 2005. Orexins cause depolarization via nonselective cationic and K+ channels in isolated locus coeruleus neurons. Neurosci. Res. 51, 55–65.

Nagai, K., Miyake, K., Kubota, T., 2005. A transcriptional repressor MeCP2 causing Rett syndrome is expressed in embryonic non-neuronal cells and controls their growth. Brain Res. Dev. Brain Res. 157, 103–106.

Perry, T.L., Dunn, H.G., Ho, H.H., Crichton, J.U., 1988. Cerebrospinal fluid values for monoamine metabolites, gamma-aminobutyric acid, and other amino compounds in Rett syndrome. J. Pediatr. 112, 234–238.

Qian, X., Shen, Q., Goderie, S.K., He, W., Capela, A., Davis, A.A., Temple, S., 2000. Timing of CNS cell generation: a programmed sequence of neuron and glial cell production from isolated murine cortical stem cells. Neuron 28, 69–80.